An unusually powerful mode of low-frequency sound interference due to defective hair bundles of the auditory outer hair cells

Kazusaku Kamiya, Vincent Michel, Fabrice Giraudet, Brigitte Riederer, Isabelle Foucher, Samantha Papal, Isabelle Perfettini, Sébastien Le Gal, Elisabeth Verpy, Weiliang Xia, et al.

An unusually powerful mode of low-frequency sound interference due to outer hair cell hair bundle defects unveiled in *Nherf1*$^{-/-}$ mice

Kazusaku Kamiya[a,b,c,d,1], Vincent Michel[a,b,c,1], Fabrice Giraudet[e], Brigitte Riederer[f], Isabelle Foucher[a,b,c], Samantha Papal[a,b,c], Isabelle Perfettini[a,b,c], Sebastien Le Gal[a,b,c], Elisabeth Verpy[a,b,c], Weiliang Xu[f], Ursula Seidler[f], Maria-Magdalena Georgescu[g], Paul Avan[e,2], Aziz El-Amraoui[a,b,c,2], and Christine Petit[a,b,c,h,2]

[a] Institut Pasteur, Génétique et Physiologie de l'Audition, 75015 Paris, France

[b] INSERM UMRS 1120, Paris, France

[c] Sorbonne Universités, UPMC Univ Paris06, Paris, France

[d] Juntendo University School of Medicine, 1138421 Tokyo, Japan

[e] Laboratoire de Biophysique Sensorielle, INSERM UMR 1107, Faculté de Médecine, Université d'Auvergne; 63000 Clermont-Ferrand, France

[f] Hannover Medical School, GHE department, Hannover, Germany.

[g] Department of Neuro-Oncology, Anderson Cancer Center, Houston, USA

[h] Collège de France, Paris, France

Short title: Inordinate low-frequency masking in *Nherf1*$^{-/-}$ mice

Keywords: Nherf1, PDZ domain, off-frequency detection, hair bundle, hearing impairment

Author contributions: P.A., A.E., and C.P. designed research; K.K., V.M., F.G., B.R., I.F., S.P., I.P., S.L., E.V., and W.X. performed research; K.K., V.M., P.A., A.E., and C.P. analyzed data; U.S. and M.M.G. contributed reagents, and P.A., A.E., and C.P. wrote the paper.

[1] Contributed equally to this work

[2] Co-senior and corresponding authors:

aziz.el-amraoui@pasteur.fr; christine.petit@pasteur.fr

Unité de Génétique et Physiologie de l'Audition, INSERM UMRS 1120, Institut Pasteur, 25 rue du Dr Roux, 75015 Paris, France

paul.avan@udamail.fr

Laboratoire de Biophysique Sensorielle, Faculté de Médecine, Université d'Auvergne, 63001 Clermont-Ferrand, France

Abstract

A detrimental perceptive consequence of damaged auditory sensory hair cells consists in a pronounced masking effect exerted by low-frequency sounds, thought to occur when auditory threshold elevation substantially exceeds 40 dB. Here, we identified Nherf1, a PDZ domain-containing protein as a hair-bundle component of the differentiating outer hair cells (OHCs). *Nherf1*$^{-/-}$ mice displayed OHC hair-bundle shape anomalies in the mid and basal cochlea, normally tuned to mid- and high-frequency tones, and mild (22-35 dB) hearing-threshold elevations restricted to mid-high sound frequencies. This mild decrease in hearing sensitivity was, however, discordant with almost non-responding OHCs at the cochlear base as assessed by distortion-product otoacoustic emissions and cochlear microphonic potentials. Moreover, unlike wild-type mice, responses of *Nherf1*$^{-/-}$ mice to high-frequency (20-40 kHz) test tones were not masked by tones of neighboring frequencies. Instead, efficient maskers were characterized by: *i)* their frequencies up to two octaves below the probe-tone frequency, *ii)* unusually low intensities, up to 25 dB below probe-tone level, and *iii)* growth-of-masking slope (2.2 dB per dB) reflecting their compressive amplification. Together, these properties do not fit the current acknowledged features of a hypersensitivity of the basal cochlea to lower frequencies, but rather suggest a novel mechanism. Low-frequency maskers, we propose, may interact within the unaffected cochlear apical region with mid-high frequency sounds propagated there via a mode possibly using the persistent contact of misshaped OHC hair-bundles with the tectorial membrane. Our findings thus reveal a novel source of misleading interpretations of hearing thresholds and of hypervulnerability to low-frequency sound interference.

Significance

We show that Nherf1 is necessary for the correct shaping of the stereocilia-bundle of outer hair cells in the basal cochlea. The mild elevation of hearing thresholds of *Nherf1*$^{-/-}$ mice at high frequencies (22-35 dB) were inconsistent with the almost total loss of outer hair cells functionality in the basal cochlea. Responses of *Nherf1*$^{-/-}$ mice to high-frequency (20-40 kHz) test-tones were masked by tones displaying inordinate characteristics in frequency, level and growth response. We suggest that in *Nherf1*$^{-/-}$ mice, high-frequency vibrations are detected in the unaffected apical region of the cochlea, thus accounting for the highly powerful masking effect of low-frequency sound. This novel source of misleading evaluation of high-frequency hearing thresholds and hypervulnerability to low-frequency sound interference should be systematically sought in hearing-impaired patients.

INTRODUCTION

Mammalian hearing displays remarkable sensitivity, fine temporal acuity and exquisite frequency selectivity, which contribute to auditory scene analysis and speech intelligibility. The first steps of sound processing, i.e. sound wave detection and neuronal encoding in the cochlea, are performed by two populations of hair cells, the inner hair cells (IHCs) and the outer hair cells (OHCs). These cells are sandwiched between the underlying basilar membrane (BM) and the overlying tectorial membrane (TM) (Fig. S1A). IHCs are the genuine sensory cells that transduce the sound stimuli into electrical signals in the primary auditory neurons. OHCs are mechanical effectors that amplify the sound-evoked movements of the cochlear partition, sharpen its frequency selectivity and produce waveform distortions (1, 2). A pure-tone stimulus entering the cochlea elicits a traveling wave that propagates along the BM from the cochlear base towards its apex, increasing in amplitude until it peaks at a characteristic place, where the mechanical properties of the cochlea are best tuned to the stimulus frequency. Beyond this characteristic place, the amplitude of the traveling wave declines rapidly to zero (1). The gradual changes in mechanical properties of the cochlea along the BM contribute to establishing the frequency-to-place map such that high-frequency sounds produce maximal responses in the basal region of the cochlea and low-frequency sounds propagate further towards the apex. In the normal cochlea, in response to a pure tone, a locally restricted OHC-driven active process boosts the traveling wave, and enhances and sharpens its peak, particularly at low stimulus levels. This causes compressive growth of the wave amplitude at the place tuned to its frequency (1, 2).

Single auditory-neuron tuning curves (TC) indicate the minimum intensity of a tone required to elicit a neuronal response as a function of tone frequency; they are informative about sound-frequency analysis in the cochlea. These curves display a dip at the characteristic frequency (CF) of the place where the neuron recorded is connected; this allows the frequency-to-place correspondence to be established. Furthermore, the sharpness of the dip indicates that of the frequency tuning of the innervated IHC (1). Masking TCs, which can be obtained by non-invasive techniques, also provide a reliable evaluation of cochlear frequency selectivity. They depict the minimum intensity of a masking sound required to suppress the response produced by a probe tone near its threshold of detection, as a function of masking sound frequency. The masking TC-dip corresponds to the most efficient masking effect, and lies near the CF of the cochlear place where the masker and probe sounds interact most efficiently. In the normal cochlea, this CF is close to the probe frequency. The normal masking TCs also present a secondary minimum: a broad, low-frequency segment less sensitive than the dip, called the TC tail. In the tail interval, the low frequency maskers exert their effect at the probe

CF place, but only at levels at least 40 dB higher than the intensity that confers masking at the dip frequency.

The most common consequence of OHC impairment is an increased width of TC dips and a decreased dip sensitivity, whereas the sensitivity in the interval of the tail may increase. Frequency shifts of TC dips, less common, are considered to reflect off-frequency hearing (3, 4), a condition reported in patients with dead cochlear zones defined as cochlear intervals in which IHCs and/or associated neurons are non-functional. However, intense sound stimulations may be detected in cochlear regions adjacent to dead zones, inferred from the position of where the masking-TC dips have shifted (4). About 60 % of deaf people with a hearing threshold above 70 dB have cochlear dead regions (4).

Perturbed frequency selectivity leads to substantial difficulties in understanding speech. Its detection in hearing-impaired individuals is therefore essential and appropriate patient management requires its origin to be determined. This would also help clarifying the involvement of the various cochlear structures in sound processing and the way they interplay in both normal and pathological conditions. Here, we report a study of the mouse mutant *Nherf1*$^{-/-}$ defective for Nherf1 (Na^+-H^+ exchanger regulatory factor 1), a PDZ domain-containing protein abundant in the OHC hair bundles. Morphological analysis showed hair bundles anomalies of OHCs in the basal, but not apical, region of the cochlea. Electrophysiological investigations revealed an interference, with inordinate characteristics, of low-frequency sounds with the response to high-frequency sounds. The current models of intense low-frequency interference cannot explain these characteristics. We propose an alternative explanation of the extreme vulnerability of *Nherf1*$^{-/-}$ mice to low-frequency sounds.

RESULTS

Nherf1, a PDZ domain-containing protein that is abundant in the OHC hair bundle

Slc9a3r1 (solute carrier family 9, member 3, regulatory 1) transcripts were identified in a subtracted cDNA library designed to search for proteins preferentially or specifically expressed in sensory epithelia of the inner ear. *Slc9a3r1* encodes Nherf1 (also called Ezrin-radixin-moesin-binding protein of 50 kDa, Ebp50), a member of the Nherf protein family (Fig. S2A,B) that consists of four PDZ domain-containing adaptor proteins present in most polarized epithelial cells. In parallel, our work with the yeast two-hybrid system to search for partners interacting with key components of the hair bundle identified Nherf1 as possibly binding to the cytodomain of cadherin-23 (Fig. S2A). Cadherin-23 forms both the transient early lateral links that connect stereocilia to each other and to the kinocilium, and the tip-link, central to the gating of the mechanoelectrical transduction channels (Fig. S1B). Colocalization and co-immunoprecipitation experiments provided further evidence for an interaction between Nherf1 and cadherin-23 (Fig. S2C-F).

The spatiotemporal distribution of Nherf1 in wild-type mice was analyzed using anti-Nherf1 specific antibodies (Figs. 1A-C, S3A). On embryonic day 15.5 (E15.5), Nherf1 was detected in stereocilia as they emerged at the apical surface of the differentiating hair cells in the basal region of the cochlea (Fig. S3B). As development proceeded, Nherf1 immunostaining increased in the hair bundles of IHCs and OHCs, with the labeling intensity increasing from the cochlear base to apex (Fig. 1A). By E17, Nherf1 was detected in the hair bundles of all hair cells, throughout the cochlea (Fig. S3B). The labeling was most intense at the tips of the stereocilia (Fig. S3C). At post-natal (P) stages, Nherf1 was no longer detected in IHC hair bundles, whereas the labeling intensity in the OHC hair bundles continued to increase up to P5, and declined from P10 onwards (Figs. 1A, S3B). Nherf1 and cadherin-23 were both present at the tips of stereocilia in the differentiating OHC hair bundles (Fig. 1B), and Nherf1 immunoreactivity was substantially lower in cadherin-23 deficient (*Cdh23*$^{v2j/v2j}$) than control mice (Fig. 1C), which is consistent with the two proteins interacting also *in vivo*.

OHC hair bundles from *Nherf1*$^{-/-}$ mice display a base-to-apex gradient of abnormal shapes

Scanning electron microscopy analysis of the differentiating and mature cochlea in *Nherf1*$^{-/-}$ mice showed major hair bundle anomalies in OHCs, but not IHCs (Figs. 2, S4,5). At early (P0-P5) and later (P20 to P60) post-natal stages, the OHC hair bundles had rounded,

hooked, wavy or linear shapes (Figs. 2A,B; S4A). However, the length, and the number of stereocilia per OHC hair bundle, the regular staircase-like pattern of the stereocilia rows, and the hair-bundle links that connect the growing stereocilia, did not differ between *Nherf1*$^{-/-}$ and control mice (Figs. 2, S4B). Despite the persistence of the links between the kinocilium and adjacent stereocilia, the positioning of the kinocilia relative to their expected positions along the planar polarity axis (Figs. 2D, S4C) was abnormal in OHCs at the cochlear base in P3-P7 *Nherf1*$^{-/-}$ mice (Fig. S4C: only 26±2 % of the kinocilia at the cochlear base were present within 6° of the PCP axis, versus 58±3 % for wild-type mice). Quantitative analysis of the *Nherf1*$^{-/-}$ cochlea at P20-P25 revealed a conspicuous cochlear base-apex gradient of hair bundle shape anomalies: 80±5 %, 50±5 %, and 10±2 % of hair bundles were abnormal in the basal, middle, and apical regions of the cochlea, respectively. These anomalies were very pronounced at the base, and subtler at the apex of the cochlea (Figs. 2C, S5A-C).

In wild-type mice, the tallest stereocilia of the OHC hair bundles are anchored in the TM, where they form characteristic V-shaped imprints at its lower aspect (Fig. 2D). These imprints provide a well-defined overall view of the shape of the OHC hair bundle's anchor in the TM. In *Nherf1*$^{-/-}$ mice, these imprints were present, but they were severely mis-shaped for 90±5 % of OHCs at the cochlear base and only affected, and less strongly so, for 15±3 % of OHCs at the apex (Figs. 2D, S5D). Antibodies directed against stereocilin, a protein present at the interface between the tips of the tallest stereocilia of the OHCs and the TM, labeled the stereocilia imprints in the TM (Figs. 2D, S5E). This confirms that the anchoring of these stereocilia in the TM was normal, despite the abnormal shapes of the hair bundles.

In *Nherf1*$^{-/-}$ mice, mild mid-high frequency threshold elevation contrasts with severely defective responses of the OHCs at the cochlear base

We next analyzed the hearing sensitivity of *Nherf1*$^{-/-}$ mice at P21-P25 by measuring the thresholds of distortion-product otoacoustic emissions (DPOAEs) and auditory brainstem responses (ABR) to brief pure-tone stimuli in the 5-40 kHz frequency range (Fig. 3). There was no significant difference in DPOAE thresholds between *Nherf1*$^{-/-}$ (n=11) and wild-type (n=11) mice for primary tone frequencies in the 5-15 kHz range ($p>0.99$; Figs. 3A, S6A). By contrast, between 19 and 28 kHz, DPOAE thresholds in *Nherf1*$^{-/-}$ mice were higher than normal and approached the upper limit of detectability (Figs. 3A, S6A), and DPOAEs were undetectable at 32 kHz in all mutant mice (Fig. 3B). The corresponding DPOAE threshold elevations were 29.7±14 dB at 20 kHz and >47.5 dB at 32 kHz ($p<0.0001$; Fig. 3A). We also measured the cochlear microphonic potential (CM), which, being proportional to the sound-induced

transducer potentials of the OHCs of the basal-most cochlear region, is an indicator of their mechano-electrical transduction (5): the mean CM was 10 times smaller in *Nherf1*$^{-/-}$ mice (n=10) than in wild-type mice (n=10) ($p<0.05$, Fig. 3C), indicating a drastic decrease of OHC function in the cochlear base. The ABR thresholds of *Nherf1*$^{-/-}$ mice were within the normal range for tone-burst frequencies below 15 kHz ($p>0.05$ at 15 kHz), consistent with the normal DPOAEs in the low-frequency interval. Above 15 kHz, ABR thresholds were only moderately higher than in control mice (by 22.2±10 dB at 20 kHz and 35±12 dB between 32 and 40 kHz, $p<0.0001$) (Fig. 3D), at odds with the DPOAE defects.

We analyzed the latencies of the first peak of the compound action potential (CAP) and its ABR wave-I correlate, which reflect the synchronous response of the auditory nerve to tone bursts. They depend on the propagation delay of the wave associated with the stimulus to the responding cochlear site. They also include intensity-dependent contributions from the local processing mechanisms in the sensory cells. In wild-type mice, CAP latencies in response to a 10 kHz probe were between 2.02 ms at the ABR threshold and 1.28 ms at 105 dB SPL; at 32 kHz, the range was from 1.70 ms at the ABR threshold to 1.15 ms at 105 dB SPL (n=10) (Fig. 3E). The difference in CAP latencies at a given sound level between 10 kHz and 32 kHz was consistent with the base-to-apex cochlea frequency map. In *Nherf1*$^{-/-}$ mice (n=10), the CAP latency plot at 10 kHz was similar to that for control mice ($p>0.85$, Fig. 3E): at 32 kHz, the CAP latency was between 1.97 and 1.31 ms, and thus in the same range as for 10 kHz tone-bursts (Figs. 3E; S6B). Even at stimulus levels of 95 ($p<0.01$) and 105 ($p<0.05$) dB SPL, such that OHC function negligibly influences the timing and size of cochlear responses, CAP latency at 32 kHz remained at least 0.18 ms longer in *Nherf1*$^{-/-}$ than control ears (Figs. 3E; S6B).

Masking tuning curves for mid-high frequency sounds display major shifts towards low frequencies in *Nherf1*$^{-/-}$ mice

To examine further the functional status of basal OHCs in *Nherf1*$^{-/-}$ mice, masking TCs were used to measure their frequency selectivity (Fig. 4). Masking TCs show how the relative frequency distance between masker and probe frequencies shapes their interaction at the cochlear site where this interaction, and thus the masking effect, occurs. Probe frequencies were set either at 10 kHz, a frequency with normal ABR hearing thresholds (Fig. 3A,D), or between 20 and 40 kHz corresponding to frequencies at which cochlear responses were clearly affected in all *Nherf1*$^{-/-}$ mice (Fig. 3A,D). In the normal cochlea, the masking-TC dip lies close to that of the probe tone at the CF of the cochlear place at which the masker and probe tones

interact most efficiently, irrespective of the tested probe frequency (10, 27, 32, or 40 kHz; Fig. 4A). In *Nherf1*$^{-/-}$ mice at 10 kHz (n=12), masking TCs displayed a narrow dip near the probe frequency and a broad low-frequency tail, almost superimposed on those in *Nherf1*$^{+/+}$ (n=12) mice (Fig. 4A). By contrast, for probe frequencies equal to or above 20 kHz (n=33), the masking TCs in *Nherf1*$^{-/-}$ mice were markedly abnormal: there were few dip-like minima around the probe frequency (Figs. 4A,B, S7A) and only for masker intensities exceeding 100 dB SPL (Fig. S7A, right panel). Conversely, intense masking was systematically observed for masker tones of lower frequencies, with a mean of 12.7±5.3 kHz, such that the most efficient masker was 2.15 octaves below the probe with the highest frequency tested (40 kHz).

Our calibration of the acoustic setup (Fig. S8A), and the masking TCs obtained in *Nherf2*$^{-/-}$ mice (Figs. 4C, S8, S9), defective for another member of the Nherf protein family, rule out any possibility of participation of the spectral splatter to the shift of masking toward low-frequency sounds. The low-frequency minimum of masking TCs in *Nherf1*$^{-/-}$ mice peaked for masker levels a mean of 15±11 dB lower than the probe tone, in some cases 25 dB lower (Fig. 4A,B). In each mutant, the frequency interval of this efficient masking was within the frequency range of its normal ABR and DPOAE thresholds (red background in Figs. 4A,B, S7A). For any single ear, masking TCs with probes of different frequencies between 20 and 40 kHz, such that DPOAE thresholds at these frequencies exceeded 70 dB (n=7), systematically coincided within 5 dB of each other over the whole frequency range of tested maskers (Figs. 4B, S7A).

In normal healthy ears, maximum masking occurs when the frequency of at least one of the two interfering sounds, the probe or the masker, coincides with the CF of the cochlear place where the masking effect is generated (2, 4, 6). In an active cochlea, the BM vibration for intermediate stimulus intensities (20-80 dB SPL) undergoes compressive amplification of its displacements solely at the CF place of the stimulus, where it increases by only about 0.3 dB per dB increase of sound level in the ear canal. By contrast, cochlear vibrations at places distant from the CF place, not influenced by OHC activity, increase linearly by 1 dB per dB (1). Which of the two sounds is at CF at the interference place should be revealed by its compressive behavior; this can be determined by measuring the increase of the masker intensity with increasing probe intensity (growth of masking, GOM) (6).

In wild-type mice, when probe and masker frequencies were close to each other (20 and 19 kHz, or 32 and 30 kHz, respectively), a paradigm referred to as 'on-frequency' masking, the GOM was about 1 dB per dB (Fig. S7B): both the probe and masker cochlear responses displayed similar compressed rates of increase at their interference place (20 kHz or 32 kHz CF

place, respectively) (6). In *Nherf1*$^{-/-}$ mice with normal ABRs at 10 kHz, a frequency at which on-frequency masking was efficient, the GOM was also about 1 dB per dB (Figs. 4D, S7B).

We then examined masking when probe and masker are set at very different frequencies, e.g., 32 and 12.5 kHz respectively, referred to as 'off-frequency' masking. In *Nherf1*$^{+/+}$ mice, the GOM was 0.35 dB per dB (n=10) for probe intensities between 30 and 65 dB SPL (Fig. 4D), and was slightly steeper above 65 dB SPL. This is coherent with the reported decrease in compression at increasing levels (1). In *Nherf1*$^{-/-}$ mice (n=12), the pattern of masker growth under the same stimulation conditions was reversed: the GOM was 2.2 dB per dB for probe intensities in the 50-65 dB SPL range (Fig. 4D). This inversed pattern indicates that the efficient low-frequency maskers undergo more compression than the probe sound that they mask, suggesting that maskers act near their own CF place. This raises questions about the idea that in the 50-65 dB SPL range (Fig. 4D), the place where the high-frequency probe stimulus elicits its CAP has a high CF (Table S1).

DISCUSSION

The hearing impairment in *Nherf1*$^{-/-}$ mice is characterized by a transition between normal low-frequency responses, below 15 kHz, and abnormal high-frequency responses above 15 kHz (Fig. 3A, C). Consistent with this, anomalies of OHC hair bundles are rare at the cochlear apex, more prevalent in the middle region of the cochlea, and involve 95% of OHCs at the cochlear base. The lack of Nherf1-mediated structural and signaling activities in these mutant mice probably results in slackening of stereocilia membrane tension, as suggested by the irregular shapes of OHC hair bundles. During hair bundle differentiation, cell intercalations and cell-cell junction remodeling concomitant with the convergent extension process are conspicuous at the cochlear base but are rare at the apex. This may explain the gradient of the prevalence of anomalies increasing from apex to base. The absence of high-frequency DPOAEs and the about 10 fold reduction of CM potential amplitude in *Nherf1*$^{-/-}$ mice indicate an overall lack of activity of the basal OHCs. This is not consistent with the small magnitude of ABR threshold elevations above 20 kHz. The OHCs are believed to influence the sensitivity of the cochlear response by acting in a feedback loop, which amplifies cochlear vibrations, by up to 60 dB, when cycle-by-cycle OHC feedback occurs with the appropriate timing. Accordingly, a 60 dB increase in ABR thresholds in the high frequency range was expected in *Nherf1*$^{-/-}$ mice (1), such that the increase of 22-35 dB that was observed was surprising (Fig. 3).

The apparent mildness of ABR threshold shifts in *Nherf1*$^{-/-}$ mice is also inconsistent with the substantial abnormality of their frequency selectivity. Modified masking TCs such that maximally efficient masking frequencies are below the probe frequency have already been reported in two conditions: the so-called “hypersensitivity of the tail” (7), and “off-frequency detection” (4).

In the “hypersensitivity of the tail” cases, TCs of individual auditory neurons innervating IHCs at cochlear places where OHCs stereocilia or these cells themselves are absent, have no sensitive dip at CF and display abnormally great sensitivity in response to low frequencies (7). This hypersensitivity is attributed to increased shear motion of the TM, due to slackened coupling to the organ of Corti in the absence of functional OHC; this is believed to confer on the basal cochlea an increased sensitivity to low frequency vibrations (7). Comparison of abnormal neuronal TCs and normal reference TCs at similar CFs show that low-frequency responses emerge in such situations at levels 10-15 dB lower than normal (7-9). In the less severe condition in which OHCs are damaged yet still present, the dips of neuronal TCs are found near the normal CF and low-frequency tails with increased sensitivity are usually observed, the tail minimum being at about the same level as the dip. However, several of our

experimental findings in *Nherf1*$^{-/-}$ mice are not coherent with this established model. First, the masking of high-frequency probes by low-frequency maskers in *Nherf1*$^{-/-}$ mice is much stronger than reported for cases ascribed to hypersensitivity of the tail. Low-frequency maskers at levels 15 dB and sometimes 25 dB below the probe level on average exerted effective masking in *Nherf1*$^{-/-}$ mice, whereas tail levels for low-frequency interference in cases of hearing loss of other types are between 15 and 25 dB higher than the probe level (Figs. 4C, S8C); in cases of hypersensitivity of the tail as described elsewhere, masking should not occur at levels lower than probe level. Second, the frequency interval at which a hypersensitive tail is found should relate directly to the mechanical coupling of the TM to OHCs at the probe-CF place, where CAP responses to the probe are elicited. This is not the case in *Nherf1*$^{-/-}$ mice, in which probe frequencies could vary from 20 to 40 kHz with no influence on TC shapes or dip positions. Indeed, the TC shapes in a given ear seemed to be related to the low-frequency interval of normal auditory sensitivity in that ear. Thirdly, according to the hypersensitivity of the tail hypothesis, low frequencies exert their masking effect at the CF place of the high-frequency probe. Whether or not OHCs are functional or not, it is generally believed that vibrations, far from their own CF place, can undergo neither amplification nor compression (1), and therefore the expected GOM should be lower than 1 dB per dB. It does not appear possible to reconcile the observed GOM in *Nherf1*$^{-/-}$ mice with this interpretative model. Finally, unlike in the case of the hypersensitivity of the tail (7), *Nherf1*$^{-/-}$ OHC hair bundles in are still anchored in the TM.

The other hypothesis, off-frequency detection, mirrors the hypersensitivity of the tail model by positing that high-frequency probes near their ABR threshold (at levels < 65 dB SPL) are not detected at the place tuned to the probe itself but at the CF places of best maskers, i.e., within the normally sensitive and immediately apical cochlear region. In the typical case of a dead basal cochlear region, high-frequency probes are indeed detected at sensitive places not tuned to those probes but adjacent to the dead cochlear region (4). In *Nherf1*$^{-/-}$ mice, the GOM data in off-frequency settings show a 2.2 dB per dB slope, which indicates that the maskers, but not the probes, undergo compression; this implies that the places where masking occurs also actively process masker-induced vibrations (1) (Table S1). The unusual ability of low-frequency maskers to act at levels up to 25 dB lower than the detection threshold of the high-frequency probe provides further support to the notion that the probe is detected at places where the masker is amplified. In the case of dead cochlear regions, sensitive places just apical to a dead zone can still be reached by the traveling BM wave, but the probe intensity would usually have to exceed 70 dB SPL to overcome the strong apical-ward attenuation beyond the CF place (70 dB/octave; (10)). In *Nherf1*$^{-/-}$ mice, the masking TC dips could shift downward by

up to two octaves with neural responses to 32 or 40 kHz probe tone-bursts at 60 dB SPL being masked optimally by masker tones at 10-12 kHz (Fig. 4A), thus raising the critical issue of how high frequency vibrations could have reached the apical detection site as they could not have traveled along the BM. A mechanism of apical propagation other than Békésy's BM traveling wave is presumably therefore operating in *Nherf1*$^{-/-}$ mice. This mechanism differs by its ability to spread medium-level high-frequency vibrations toward the cochlear apical region. Various modes of vibration have been detected in the cochlea, and they include a fast acoustic-pressure wave traveling in cochlear duct fluids (11), but which has little effect on hair bundle deflection. The latencies of the high-frequency ABRs of *Nherf1*$^{-/-}$ mice, if produced off-frequency by an acoustic-pressure wave, should be as short as in *Nherf1*$^{+/+}$ mice. The Reissner membrane has recently been described to support the propagation of vibrations that contribute significantly to the excitation of the apical-most part of the cochlea (12). Recent *ex vivo* investigations of the viscoelastic properties of the TM suggest that it is possible for a wave to travel longitudinally along this membrane (13-15). If the *in vivo* properties are similar to those reported *ex vivo*, the features of the TM wave might allow it to propagate high-frequency vibrations to the apex of *Nherf1*$^{-/-}$ cochleas. IHC excitation requires the deflection of stereocilia bundles, and TM vibrations may cause such deflection even when the BM and reticular lamina do not vibrate.

How can high-frequency waves propagate along the TM from basal places? *Nherf1*$^{-/-}$ mice have normal numbers of OHCs in the basal region that, strikingly, display persistent mechanical coupling to the TM (Fig. 2). Consequently, passive vibrations of the basal BM might be transmitted to the TM. Normally, vibrations of the reticular lamina differ in amplitude and timing from those of the BM and both display rapid phase changes in the longitudinal direction near CF, due to OHC mechanical feedback (16); this likely hampers the efficacy of any leak to the TM in wild-type conditions. In *Nherf1*$^{-/-}$ mice with defective basal OHCs, one would expect BM motion, although weak, to occur in phase with the reticular lamina over a broad region, which may act as a beamforming mechanism resulting in significant TM motion. *Ex vivo*, TM waves undergo little attenuation over hundreds of μm and travel at 3-6 m/s, in a smooth frequency- and place-dependent manner (13). This would translate into a ~0.4-ms travel time between the places with CFs at 40 and 10 kHz, which is consistent with the observed shift in wave-I latencies of ABRs to high-frequency tone-bursts in *Nherf1*$^{-/-}$ mice (Fig. 3E). The off-frequency detection model would also account for the need for on-frequency maskers to be about 40 dB more intense than the 20 and 32 kHz probes, because the interaction between these probes and maskers is assumed to occur apically at places tuned to the best maskers, and which respond nonlinearly only to sounds near their CF. The only possible masking mechanism would be the line-busy mechanism by which the masker saturates the

neuronal activity and swamps the transient probe-induced activity (17); this requires the masker to be about 40 dB more intense than the probe.

In summary, the off-frequency detection mechanism can account for the results we report in *Nherf1*$^{-/-}$ mice without any need for altering the basic tenets of cochlear mechanics. We propose that a mode of propagation along the TM that has been described *in vitro* may extend abnormally in the apical direction *via* the persisting coupling between inactive OHCs and the TM. In patients with a similar abnormality, this would bias the interpretation of audiometric evaluation by suggesting a misleadingly mild high-frequency hearing impairment. This would in turn affect the hearing-aid fitting procedure. The detection of medium-level high-frequency sounds despite a severely damaged cochlear base may provide a beneficial natural frequency transposition, akin to that implemented by hearing aids that numerically displace inaudible high-frequency components to a mid-frequency interval to which the ear remains more sensitive. However, our findings in *Nherf1*$^{-/-}$ mice suggest that transposed information is so vulnerable to interference from low-frequency sounds that patients are likely to have major difficulties hearing in noisy environments, inconsistent with a hearing impairment misdiagnosed as 'mild'. Therefore, screening for this newly identified type of cochlear dysfunction is essential for appropriate clinical evaluations of patients with hearing disorders. Our study indicates that this problem could be identified by systematic screening for inconsistency between ABR and DPOAE measurements, and that abnormal psychophysical masking test results would reveal the unusual detrimental impact of low-frequency sounds. Finally, this work identifies two new mouse deafness genes, *Slc9a3r1* (Nherf1) and *Slc9a3r2* (Nherf2), which are likely to be responsible for hearing impairment also in humans.

Materials and methods

A detailed description of the methods is available in supplementary data. *Nherf1*$^{-/-}$, *Nherf2*$^{-/-}$, and *Cdh23*$^{v2j/v2j}$ mice were used. Immunofluorescence analysis, study of the structure of the auditory hair cells by light and scanning electron microscopy, and the *in vivo* measurements for physiological analysis were performed (see supplementary data). Experiments with animals were carried out using protocols approved by the Animal Use Committee of INSERM and Institut Pasteur.

Acknowledgments

We thank Hardelin J-P and Boutet de Monvel J for their suggestions on the manuscript, Delmaghani S, Weil D, and Muraki M for their assistance. This work was supported by Japan Society for the Promotion of Science and Uehara Memorial Foundation to KK, ERC-Hair bundle (ERC-2011-ADG_20110310), LABEX Lifesenses [ANR-10-LABX-65], Réunica-Prévoyance, Novalis-Taitbout, Errera Hoechstetter, and Fondation Voir et Entendre to CP.

References

1. Robles L & Ruggero MA (2001) Mechanics of the mammalian cochlea. *Physiol Rev* 81:1305-1352.
2. Avan P, Büki B, & Petit C (2013) Auditory Distortions: Origins and Functions. *Physiol rev* 93:1563-1619.
3. O'Loughlin BJ & Moore BC (1981) Off-frequency listening: effects on psychoacoustical tuning curves obtained in simultaneous and forward masking. *J Acoust Soc Am* 69:1119-1125.
4. Moore BC & Alcantara JI (2001) The use of psychophysical tuning curves to explore dead regions in the cochlea. *Ear Hear* 22:268-278.
5. He W, Porsov E, Kemp D, Nuttall AL, & Ren T (2012) The group delay and suppression pattern of the cochlear microphonic potential recorded at the round window. *PLoS One* 7:e34356.
6. Plack CJ & Oxenham AJ (1998) Basilar-membrane nonlinearity and the growth of forward masking. *J Acoust Soc Am* 103:1598-1608.
7. Liberman MC & Dodds LW (1984) Single-neuron labeling and chronic cochlear pathology. III. Stereocilia damage and alterations of threshold tuning curves. *Hear Res* 16:55-74.
8. Dallos P & Harris D (1978) Properties of auditory nerve responses in absence of outer hair cells. *J Neurophysiol* 41:365-383.
9. Versnel H, Prijs VF, & Schoonhoven R (1997) Auditory-nerve fiber responses to clicks in guinea pigs with a damaged cochlea. *J Acoust Soc Am* 101:993-1009.
10. Richter CP, Evans BN, Edge R, & Dallos P (1998) Basilar membrane vibration in the gerbil hemicochlea. *J Neurophysiol* 79:2255-2264.
11. He W, Fridberger A, Porsov E, Grosh K, & Ren T (2008) Reverse wave propagation in the cochlea. *Proc Natl Acad Sci USA* 105:2729-2733.
12. Reichenbach T, Stefanovic A, Nin F, & Hudspeth AJ (2012) Waves on Reissner's membrane: a mechanism for the propagation of otoacoustic emissions from the cochlea. *Cell Rep* 1:374-384.
13. Ghaffari R, Aranyosi AJ, & Freeman DM (2007) Longitudinally propagating traveling waves of the mammalian tectorial membrane. *Proc Natl Acad Sci USA* 104:16510-16515.
14. Ghaffari R, Aranyosi AJ, Richardson GP, & Freeman DM (2010) Tectorial membrane travelling waves underlie abnormal hearing in Tectb mutant mice. *Nat Commun* 1:96.
15. Lamb JS & Chadwick RS (2011) Dual traveling waves in an inner ear model with two degrees of freedom. *Phys Rev Lett* 107:088101.
16. Chen F*, et al.* (2011) A differentially amplified motion in the ear for near-threshold sound detection. *Nat Neurosci* 14:770-774.
17. Delgutte B (1996) Physiological models for basic auditory percepts. *Auditory Computation*, eds Hawkins HH, Mc Mullen TA, Popper AN, & Fay RR (Springer, New York), pp 157-220.

Figure legends

Fig. 1: Nherf1 in the mouse auditory hair cells

(A) Nherf1 immunostaining is detected on embryonic day 16 in the stereocilia of IHCs and OHCs. After birth (P0 and P12), Nherf1 was detected only in OHC hair bundles. Nherf1 labeling was intense at the tips of the differentiating stereocilia. (B) Nherf1 and cadherin-23 colocalized at the stereocilia tips. (C) On P5, Nherf1 labeling was weaker in the stereocilia of hair cells, but not in the supporting cells (arrows in B and C), in *Cdh23*$^{v2j/v2j}$ mice than in controls. Bars=5 μm.

Fig. 2: Abnormal OHC hair bundle shapes in *Nherf1*$^{-/-}$ mice

(A,B) In *Nherf1*$^{-/-}$ mice, the shapes of the OHC hair bundles are abnormal mainly in the basal cochlear region: wavy, linear and hooked shapes are observed. (C) Abnormally shaped OHC hair bundles (light and dark greens, lower panels) and normal, V-shaped hair bundles (blue) were counted in each cochlear region (basal, middle, apical) in *Nherf1*$^{-/-}$ and wild-type mice: in *Nherf1*$^{-/-}$ mice, 80±5 % of OHCs in the cochlear basal region displayed abnormal hair bundle shapes. (D) In *Nherf1*$^{-/-}$ mice (lower panels), OHC imprints on the TM at the cochlear base (also labeled by anti-stereocilin antibodies, green) predominantly correspond to mis-shaped arrays of OHC stereocilia. Bars=1 μm.

Fig. 3: Hearing impairment at mid-high sound frequencies in *Nherf1*$^{-/-}$ mice

(A-D) DPOAEs, CM potentials, and ABRs in P20-P25 wild-type (black), and *Nherf1*$^{-/-}$ (red) mice. (A) DPOAE thresholds (±sd) at and above 20 kHz are significantly higher in *Nherf1*$^{-/-}$ mice than in wild-type mice. (B) The DPOAEs (±sd) at 32 kHz are indistinguishable from noise background in *Nherf1*$^{-/-}$ mice (red, downward-pointing arrows; n=11). In these cases, DPOAE thresholds were arbitrarily set at 75 dB SPL, the highest intensity stimulus tested. (C) The amplitude of the CM potential for a 10 kHz tone burst stimulus (±sem), measured at the round window, was significantly smaller in *Nherf1*$^{-/-}$ mice (n=10) than in control (n=10) mice. (D) Beyond 15 kHz, the ABR thresholds (±sd) were significantly higher in *Nherf1*$^{-/-}$ mice than

in control littermates. (E) ABR wave-I timing at 10 and 32 kHz as a function of stimulus sound level in *Nherf1*$^{-/-}$ mice**.** For 10 kHz tone-burst sound stimuli, average ABR wave-I latencies (±sd) did not differ between wild-type (black dashed line) and *Nherf1*$^{-/-}$ mice (red dashed line), regardless of the strength of the stimulus. The latency of the 32 kHz ABR-wave I for *Nherf1*$^{-/-}$ mice (red plain line) was shifted upward by 0.4 to 0.6 ms relative to that for wild-type mice (black plain line) between 45 and 85 dB SPL. *, ** and *** denote $p<0.05$, $p<0.01$ and $p<0.001$, respectively. (ns) not significant.

Fig. 4: Abnormally efficient masking of mid-high frequency sounds by lower frequency sounds in *Nherf1*$^{-/-}$ mice

(A) For a low frequency probe tone (10 kHz) (left graphs in the left panel), the masking TC recorded in a *Nherf1*$^{-/-}$ mouse did not differ from that in a wild-type mice. The most efficient masker (dip of the V-shaped curve) was at or near the probe frequency and within 10 dB of the probe intensity (see ABR thresholds curve). For mid-high frequency probe tones (27 (blue), 32 (green) and 40 (orange) kHz), the efficient masking (the dip of the TC) was shifted towards low frequency sounds (light red background), on average at 12.5 kHz in the *Nherf1*$^{-/-}$ mice (right panel). (B) Scatterplots of the most efficient masking frequency (TC dip frequency) as a function of probe frequency in wild-type (grey to black dots) and *Nherf1*$^{-/-}$ (colored dots) mice. Colored lines connect data points collected in the same ear at the different probe frequencies as indicated. In *Nherf1*$^{-/-}$ mice (n=12), the efficient masking for mid-high frequency sounds (beyond 20 kHz) was shifted towards low frequency sounds (light red background). (C) For a 20 kHz probe tone in *Nherf2*$^{-/-}$ mice, the most efficient masking (still centered near the probe frequency) was at higher levels than for wild-type mice. (D) Growth of masking (GOM) curves for off-frequency conditions (signal at 32 kHz and masker at 12.5 kHz). In the intermediate range of probe tone-burst intensities (yellow zone), the slope of the GOM curves for wild-type mice was shallow (0.35 dB per dB, n=10), and that for *Nherf1*$^{-/-}$ mice was much steeper (2.2 dB per dB, n=12). The large GOM allowed compression measurements to be made with probe tone-burst levels not exceeding 65 dB SPL (yellow zone), which kept the risk of spectral splatter under control.

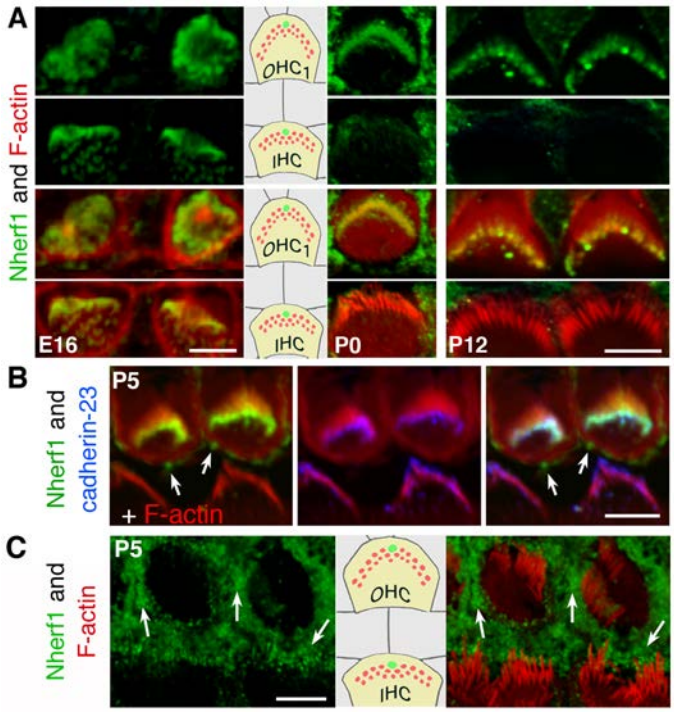
A
Nherf1 and F-actin
OHC1
IHC
OHC1
IHC
E16
P0
P12
B
Nherf1 and cadherin-23
P5
+ F-actin
C
Nherf1 and F-actin
P5
OHC
IHC

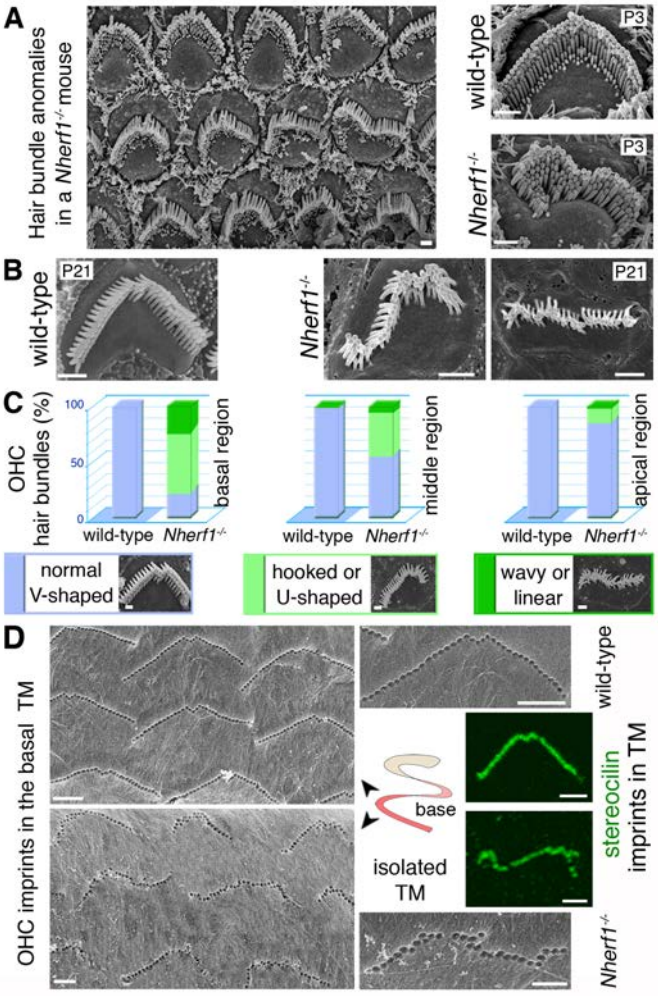
A
Hair bundle anomalies in a Nherf1-/- mouse
wild-type
P3
Nherf1-/-
P3
B
wild-type
P21
Nherf1-/-
P21
C
OHC hair bundles (%)
100
50
0
basal region
middle region
apical region
wild-type
Nherf1-/-
normal V-shaped
hooked or U-shaped
wavy or linear
D
OHC imprints in the basal TM
wild-type
base
isolated TM
stereocilin imprints in TM
Nherf1-/-

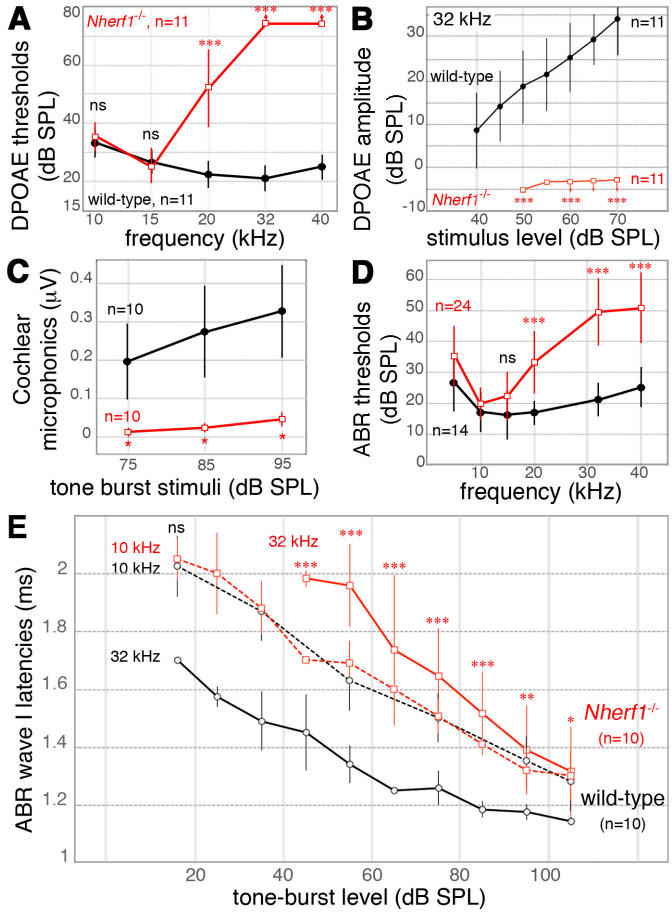
A
DPOAE thresholds (dB SPL)
Nherf1-/-, n=11
wild-type, n=11
ns
ns
***
***
***
frequency (kHz)
B
DPOAE amplitude (dB SPL)
32 kHz
wild-type
n=11
Nherf1-/-
n=11
***
stimulus level (dB SPL)
C
Cochlear microphonics (μV)
n=10
n=10
*
tone burst stimuli (dB SPL)
D
ABR thresholds (dB SPL)
n=24
n=14
ns
***
frequency (kHz)
E
ABR wave I latencies (ms)
ns
10 kHz
10 kHz
32 kHz
32 kHz
Nherf1-/-
(n=10)
wild-type
(n=10)
tone-burst level (dB SPL)

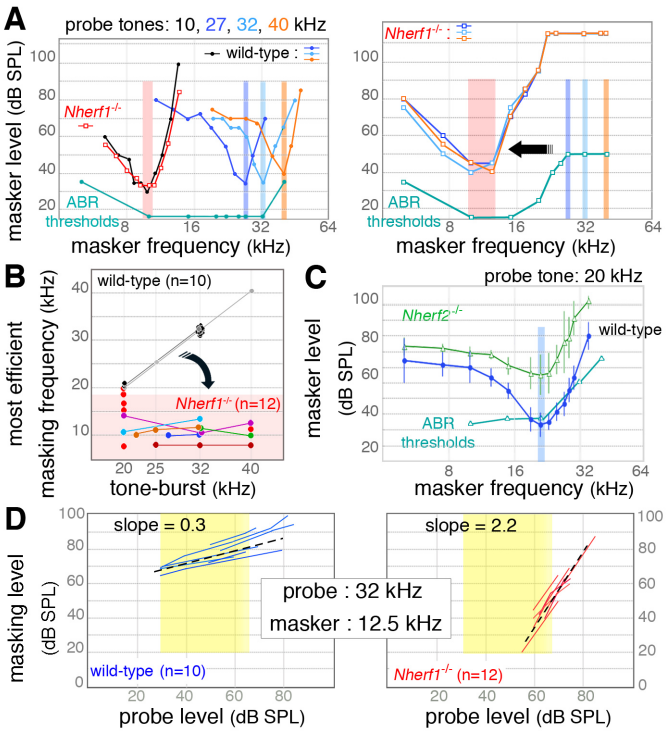
A
probe tones: 10, 27, 32, 40 kHz
wild-type :
Nherf1-/- :
Nherf1-/-
ABR thresholds
masker level (dB SPL)
masker frequency (kHz)
B
most efficient masking frequency (kHz)
wild-type (n=10)
Nherf1-/- (n=12)
tone-burst (kHz)
C
probe tone: 20 kHz
Nherf2-/-
wild-type
masker level (dB SPL)
masker frequency (kHz)
D
masking level (dB SPL)
slope = 0.3
slope = 2.2
probe : 32 kHz
masker : 12.5 kHz
wild-type (n=10)
Nherf1-/- (n=12)
probe level (dB SPL)

Kamiya K, Michel V, et al. 2014 (PNAS MS#2013-21381) SUPPLEMENTARY DATA

I- Legends to the supplementary figures S1-S9

Fig. S1: The auditory sensory organ and the hair bundle, the sound-receptive structure of sensory hair cells

(A) The inner ear (upper left panel) contains the vestibule (balance organ), and the cochlea (auditory organ). Running from the base to the apex of the cochlea, the auditory sensory epithelium lies on the basilar membrane. The lower left panel illustrates the frequency-place (tonotopic) map on an F-actin-labeled (red) mouse cochlea. In the auditory sensory epithelium (lower right panel), sensory inner hair cells (IHCs) are organized into a single medial-side row and outer hair cells (OHCs) into three lateral-side rows. A mechanosensitive hair bundle, made of 50 to 300 actin-filled rigid microvilli, known as stereocilia, crowns the apical surface of each hair cell (upper right panel). The tectorial membrane, anchored to the spiral limbus, overlies the sensory epithelium, and is in contact with the tallest stereocilia of OHCs. (B) In the developing hair bundle, a single transient primary cilium, the kinocilium, is located towards the periphery of the hair bundle, attached to adjacent stereocilia of the tallest row by the kinociliary links (KL). The stereocilia are connected by early lateral links (ELL), and ankle links (AL). These transient lateral links are subsequently replaced by the top connectors (TC) in the outer hair cells. The right panel is a magnification of the apical regions of stereocilia from the middle and tall rows of a mature hair bundle. Cadherin-23 and protocadherin-15 form the tip-link, a major component of the mechano-electrical transduction (MET) machinery. These proteins interact with other proteins —proteins including myosin VIIa, harmonin and SANS, that are defective in cases of Usher syndrome of type I— at each tip-link insertion point. The MET channels are located at the tips of stereocilia of the short and middle rows.

Fig. S2: Nherf1 and cadherin-23, the protein defective in Usher syndrome type 1D

(A) Modular structures of cadherin-23 (bait) and Nherf1 (prey). The position and domain structure of the yeast two-hybrid bait, the cytodomain of murine cadherin-23 containing the

fragment encoded by exon 68, and the three independent Nherf1-prey clones isolated are indicated. The common region of three independent prey clones (aa 1-165) is predicted to encode the N-terminal region of Nherf1/ Ebp50. Nherf1 contains two PDZ domains, an ERM-binding (EB) domain, and a C-terminal class-1 PDZ-binding motif (asterisk). (B) Nherf family members. Nherf1 belongs to a family of four PDZ domain-containing adaptors (Nherf1-Nherf4). Nherf1 and Nherf2 are both composed of two PDZ domains, and an ERM-binding domain that links the proteins to the cytoskeleton. Nherf3 and Nherf4 contain four PDZ domains without any additional regulatory or interaction domains. All Nherf proteins have a C-terminal class-1 PDZ-binding motif (asterisk). (C) Co-immunoprecipitation assays. Co-transfected HEK293 cells producing either the V5-tagged Nherf1 and myc-tagged cadherin-23 cytodomain, or the V5-tagged Nherf1 and the myc-tagged radixin were used for co-immunoprecipitation experiments. The V5-tagged Nherf1 (top) and myc-tagged cadherin-23 cytodomain were co-immunoprecipitated by the anti-V5 antibody. The Nherf1-radixin interaction serves as a positive control. (D-F) Nherf1 and the cadherin-23 cytodomain in the polarized LLC-PK-CL4 epithelial cells. (D) In co-transfected CL4 cells producing Nherf1 and the entire cytoplasmic region of cadherin-23 (Cdh23cyto), the two proteins were co-located in the apical microvilli. (E) In cells producing V5-tagged Nherf1 and a truncated form of cadherin-23 cytodomain that lacks the last nine amino acid residues (Cdh23cytoΔ9), the two proteins were not co-located; therefore the interaction probably involves the C-terminal PDZ-binding motif of cadherin-23. (F) CL4 cells were co-transfected with constructs encoding Nherf1 and an hEcadCdh23cyto chimera, composed of the five extracellular cadherin repeats (EC) and transmembrane domain (TM) of the human E-cadherin (hEcadherin) fused to the intracellular domain of the human cadherin-23 (cadherin-23cyto). In these cells, Nherf1 accumulated at the cell-cell junctions together with hEcadCdh23 (arrows), but not elsewhere at the plasma membrane (arrowheads). The schematic diagrams in (D-F) illustrate the domain structure of the fragments produced in CL4 cells. Bars=10 μm.

Fig. S3: Nherf1 spatio-temporal distribution in the auditory sensory epithelium

(A) The specificity of Nherf1 immunolabeling (green) in the hair bundles. The immunolabeling of the stereocilia observed in wild-type mice is absent from *Nherf1*$^{-/-}$ mice (right panel) and is therefore specific for Nherf1. (B) Cochlear sensory epithelia stained for Nherf1 (green) and F-actin (red). At embryonic stages (E15.5, E17, and E18), Nherf1 immunolabeling was detected in the hair bundles of both inner hair cells (IHC) and outer hair cells (OHC). At E15.5, Nherf1 was detected in the actin-rich protrusions that grow on top of

the newly differentiated hair cells; similar Nherf1 distributions were also observed at E17.5 and E18.5 in the stereocilia of IHCs, OHCs, and in the microvilli of surrounding supporting cells. On early postnatal days (P0, P3, P5), the protein was no longer detected in IHCs, but the immunoreactivity in the OHC hair bundles increased. Nherf1 immunolabeling was strong at the tips of the stereocilia. This was confirmed by post-embedding immunogold labeling experiments: on E18, the Nherf1-specific gold particles were mainly detected in the apical half of the differentiating stereocilia (upper right panel). The microvilli of surrounding supporting cells were also intense immunolabeled for Nerf1 (arrows in bottom right panel). (C) Isolated OHCs illustrating the strong Nherf1 immunolabeling in the apical regions of the stereocilia (left panels). The immunolabeling of Nherf2, another member of the Nherf family, was stronger in the stereocilia basal region (right panels).
Bars=5 μm, 250 nm (upper right panel in B).

Fig. S4: Abnormal hair bundle shapes and mispositioned kinocilium in the OHC hair bundles of *Nherf1*$^{-/-}$ mice

(A-D) Top views of cochlear whole-mounts from wild-type and *Nherf1*$^{-/-}$ mice (scanning electron microscopy). (A) The shape of OHC hair bundles in *Nherf1*$^{-/-}$ mice is severely abnormal, as shown from P3 to P8. Instead of the V-shaped hair bundles in wild-type mice (left panels in A), asymmetric OHC hair bundles, with misaligned stereocilia rows, are observed in *Nherf1*$^{-/-}$ mice. (B) Left panel: the numbers of stereocilia per OHC hair bundle were not significantly different between *Nherf1*$^{-/-}$ and wild-type animals ($p>0.05$). Right panels: the lateral links that connect adjacent stereocilia in their apical (upper) and basal (lower) parts at P3 are preserved in *Nherf1*$^{-/-}$ hair bundles. (C) Mispositioned kinocilium in the OHC hair bundles in the cochlear basal region of *Nherf1*$^{-/-}$ mice. Upper panels: The upper schematic representation illustrates hair bundle orientation and the method used to measure the angular deviation of the kinocilium with respect to the planar cell polarity (PCP) axis. TRITC-phalloidin was used to label the stereocilia (red), and an anti-acetylated tubulin antibody to label the kinocilia (green). In the scanning electron micrographs (right panels), kinocilia were artificially labeled in green to facilitate visualization. Lower panels: The mean absolute deviations (± sem) of the kinocilia in the three rows of OHCs were between 12±1° and 18±1° in *Nherf1*$^{-/-}$ mice, and between 5±1° and 9±2° in wild-type mice. In wild-type mice, 58% of the kinocilia were within 7° of the PCP axis; in *Nherf1*$^{-/-}$ mice, only 26% of the kinocilia were within 15° of the PCP axis. Bars=1 μm (A, B), 5 μm (C). ** and *** denote $p<0.01$ and $p<0.001$, respectively (Student's *t* test).

Fig. S5: Abnormal OHC hair bundle shapes and TM imprints predominate in the cochlear basal region in *Nherf1*$^{-/-}$ mice

(A-C) Various abnormal shapes of the OHC hair bundles are observed in *Nherf1*$^{-/-}$ mice: they include wavy (red), linear (yellow) and hooked (green) hair bundles. (B) Examples of wild-type and *Nherf1*$^{-/-}$ hair bundles, illustrating the anomalies of OHC, but not IHC hair bundle shapes in *Nherf1*$^{-/-}$ mice. (C) At the cochlear apex of *Nherf1*$^{-/-}$ mice, the shapes of few OHC hair bundles were affected and only mildly, whereas most of the OHC hair bundles at the cochlear base were mis-shaped. (D, E) Imprints of the tallest OHC stereocilia in the tectorial membrane (TM). (D) Upper panels: In *Nherf1*$^{-/-}$ mice, almost all of the OHC imprints (90±5 %, see lower left panels) in the lower face of the TM in the cochlear basal region were mis-shaped (green in the histograms), whereas only 15±3 % were abnormal in the cochlear apical region, and in these cases the anomalies were minor (lower right panels). (E) Labeling of the stereocilia imprints of the three OHC rows of in the TM using an anti-stereocilin antibody (green) shows the abnormal imprints in *Nherf1*$^{-/-}$ mice.
Bars=5 μm (A, C), 1 μm (B, D, E).

Fig. S6: Distortion product otoacoustic emissions (DPOAEs) and ABR recordings in *Nherf1*$^{-/-}$ mice

(A) Distortion product otoacoustic emissions (DPOAEs) in P20-P28 wild-type (black) and *Nherf1*$^{-/-}$ (red) mice. Tests were carried out before P30 to avoid any interference from age-related high frequency hearing loss. DPOAEs for 10 kHz and 20 kHz tone stimuli are shown. DPOAE amplitudes in *Nherf1*$^{-/-}$ mice, within the normal range at 10 kHz, were significantly lower than normal at 20 kHz. (ns) and *** denote no statistically significant difference, and a significant difference with $p<0.0001$, respectively (2-way ANOVA). (B) Examples of ABR recordings at 10 kHz (75 dB SPL) in a wild-type mouse, and at 32 kHz in wild-type (at 75 dB SPL) and *Nherf1*$^{-/-}$ (at 75 and 95 dB SPL) mice. The latency of the 32 kHz ABR-wave I (arrows) in the *Nherf1*$^{-/-}$ mouse jumped from 1.60 to 1.25 ms when the stimulus level increased from 75 dB SPL (light red trace) to 95 dB SPL (dark red trace), but nevertheless remained 0.20 ms longer than the wave-I latency at 32 kHz, 75 dB SPL in a wild-type ear and was more similar to the wave-I latency at 10 kHz in this control ear (blue trace).

Fig. S7: Masking tuning curves (TCs) in wild-type, *Nherf1*$^{-/-}$, and *Nherf2*$^{-/-}$ mice

(A) Examples of masking tuning curves (TCs) for 20 kHz (left panels), and 32 kHz and 40

kHz (middle panels) probe tones in P20-P25 wild-type and *Nherf1*$^{-/-}$ mice. The TCs represent, against masker frequency, the smallest intensity of the masker able to decrease by half the compound action potential elicited in the auditory nerve by a probe tone-burst at 5-10 dB above the ABR threshold. In the wild-type mouse (upper panels), the TCs display a characteristic narrow V-shaped dip corresponding to the most efficient masker tone at or near the probe frequency (20, 32 or 40 kHz), and near the probe intensity. The shallow slope of TC curves toward lower frequencies defines a broad low-frequency tail, in which masker tones have to be 30-50 dB above the probe intensity to exert masking. By contrast, in the *Nherf1*$^{-/-}$ mouse (lower panels), hardly any masking was present for masker frequencies around the probe tone at 20 kHz, 32 kHz or 40 kHz. Only in some but not all *Nherf1*$^{-/-}$ mice, a dip-like minimum around the probe frequency (32 kHz) was observed for a 32 kHz masker, but with intensities exceeding 100 dB SPL (bottom right panel). In all these mutant mice, the most efficient masker (dip of the V-shaped curve) was in the lower frequency interval, between 7 kHz and 14 kHz. The most efficient masker for both 32 kHz and 40 kHz probe tones in a given ear was at the same frequency, 12.5 kHz in the example shown in the bottom middle panel. Furthermore, the two TCs coincided within 5 dB over the whole masker-frequency range. (B) Growth of masking curves experiments. Average ratios (±sd**)** of growths of masker and probe tones (in dB per dB) in wild-type and *Nherf1*$^{-/-}$ mice, when probe and masker frequencies were similar (on-frequency) or very different (off-frequency). The on-frequency configuration cannot be tested in *Nherf1*$^{-/-}$ mice because masking starts appearing only at masker intensities > 100 dB SPL. Individual growth-of-masking plots are depicted in Fig. 4A.

Fig. S8: The acoustic source of a 32 kHz tone-burst stimulus, and the auditory characteristics and masking tuning curves in wild-type, *Nherf1*$^{-/-}$, and *Nherf2*$^{-/-}$ mice

(A) **Tone-burst stimuli at high frequencies and related spectral splatter.** We tested the acoustic source of the high-frequency probe stimuli for the presence of low-frequency spectral splatter: by eliciting ABR responses in the normally sensitive low-frequency cochlear region of *Nherf1*$^{-/-}$ mice, this could account for the observed shift of masking toward low frequencies. The frequency spectrum of a 32 kHz tone-burst measured *in situ* by a calibration microphone is represented in orange. The level of the main peak at 32 kHz serves as a reference (0 dB) for the vertical dB scale. The average difference between ABR thresholds at the measured frequency at 32 kHz in *Nherf1*$^{-/-}$ mice is presented in red, and that in the *Nherf1*$^{-/-}$ most extreme ear among those tested is in blue. Analysis of the frequency spectrum revealed a low-frequency onset artifact in the 6-14 kHz frequency interval (asterisk above orange line), 45 dB below the level

of the main 32 kHz tone-burst regardless of intensity of the sound, too small to elicit spurious ABR responses (similar data were collected at 20 kHz). Thus, the spectral splatter cannot contribute to the measured 32 kHz-ABR thresholds even at 10 kHz, at which spectral splatter remains 12 dB too weak on average (and 2-dB too weak, in the less favorable ear) to produce any ABR. When the level of the 32-kHz tone-burst is well in excess of 65 dB SPL, the small artifactual ABR contributions possibly generated in cochlear regions tuned to low frequencies are likely overwhelmed by those produced by the main tone burst at its CF place, which will be stimulated well above threshold. (B) Difference in dB between thresholds at frequencies > 15 kHz and threshold at 15 kHz, for ABR (plain lines) and DPOAEs (dashed lines), in *Nherf1*$^{-/-}$ (red lines) and *Nherf2*$^{-/-}$ (green lines) mice. The DPOAE thresholds were more severely affected in *Nherf1*$^{-/-}$ (dashed red line) than in *Nherf2*$^{-/-}$ mice (dashed green line). However, the changes in ABR thresholds at increasing tone-burst frequencies were similar in the two mouse mutants, such that they are similarly sensitive to the biasing effect on ABR thresholds of a hypothetical low-frequency spectral splatter affecting the spectra of high-frequency tone-bursts (20 kHz and above). (C) The same acoustic setup was used to establish the masking tuning curves (TCs) in *Nherf1*$^{-/-}$ and *Nherf2*$^{-/-}$ mice. Unlike the masking TC for *Nherf1*$^{-/-}$ mice (lower left panel, same as S7A), the masking TC for *Nherf2*$^{-/-}$ mice (lower right panel) was centered near the probe frequency, and all changes in their characteristics followed the conventional pattern: for a 32 kHz probe, the TC dip was enlarged and elevated but remains near the probe frequency and the low-frequency tail was sensitive as in controls. The masker threshold intensities in the tail region were about 15 dB higher than those in the dip frequency interval. These observations are consistent with acoustic calibration, and rule out any possibility of participation of low-frequency transient artifacts of the acoustic stimulus in the functional pattern and masking TCs of *Nherf1*$^{-/-}$ mice.

Fig. S9: Spatio-temporal distribution of Nherf2 in cochlear hair cells, and OHC hair bundle architecture in *Nherf2*$^{-/-}$ mice

(A) The distribution of Nherf2 in the auditory sensory organ was analyzed at embryonic and postnatal stages. Nherf2 immunostaining (green) was detected as early as embryonic day E15.5 in the emerging stereocilia of both IHCs and OHCs. The staining was more intense at post-natal stages (P0, P5, and P15, and P90), especially in the stereocilia of IHCs. Most Nherf2 staining was located in the stereocilia basal region, as shown in an IHC hair bundle at P90 (right panels). (B) The specificity of the Nherf2 immunolabeling (green) in the hair bundles (F-actin labeling, red) of the wild-type mice was confirmed by its absence from

Nherf2$^{-/-}$ mice. (C) Scanning EM analysis of the OHC hair bundles in *Nherf2*$^{-/-}$ mice. At early post-natal stages (P5-P7), the OHC hair bundle shapes in *Nherf2*$^{-/-}$ mice were approximately normal, and similar to those in wild-type mice. However, some abnormally shaped OHC hair bundles were present at post-hearing stages, as illustrated here on P21 (arrows). Despite missing or fused stereocilia in the short and middle rows of some hair bundles in P21 *Nherf2*$^{-/-}$ mice, the OHC imprints on the lower surface of the TM are roughly normal all along the cochlea (see upper right panel). Bars=1 μm.

Supplementary Table S1:

Table S1: *Nherf1*$^{-/-}$ mice, off-frequency situation, probe at 32 kHz; maximally efficient masker at ~12.5 kHz

Interpretative framework	True probe frequency	CF at place of interference	Compression of probe	Compression of masker	Expected GOM
Spectral splatter	12.5 kHz	12.5 kHz	+	+	1 dB per dB
Tail hypersensitivity	32 kHz	32 kHz	+	0	0.3 dB per dB
Off-frequency detection	32 kHz	~12.5 kHz	0	+	~ 3 dB per dB

Note: If the presumed off-frequency detection occurs over a broad cochlear region, for example because the mechanism of apical propagation at its origin has little frequency specificity, efficient maskers may act despite not corresponding exactly to the CF, as CFs in the region of interference span a broad range. Consequently, maskers would not be compressed at the maximum rate and the GOM would be less than the inverse of the

maximum compression rate, thus, < 3 dB per dB. On the basis of this reasoning, the only interpretative framework that can explain the GOM data is off-frequency detection, unless tail hypersensitivity in *Nherf1*$^{-/-}$ mice is due to a novel type of OHC dysfunction such that places with normally high CFs both respond much better to low frequencies than to the CF and actively process low-frequency sounds in such a way that compression happens at low frequencies while no longer happening at the CF. However, the currently available evidence overwhelming suggests that compression requires functionally operating OHCs and is restricted to frequencies near the CF (1).

II- Supplementary materials and methods:

Subtractive inner ear cDNA library and yeast two-hybrid screening

To isolate genes preferentially expressed in hair cells, cDNAs from the sensory epithelia of P0-P4 mouse vestibular end organs were subtracted with cDNAs from the non-sensory cartilaginous and membranous parts of the P0-P4 semi-circular canals, and with P2 liver and P15 dorsal root ganglion cDNAs; a modified RDA (representational difference analysis) technique was used as described elsewhere (2).

For the yeast-two hybrid screening, the intracellular region of cadherin-23 (NM-022124; amino acid residues 3086-354) that includes the 35 amino acid residues encoded by exon 68 was used as a bait to screen a cDNA library derived from microdissected vestibular sensory epithelia of P2 to P6 mice (3).

DNA constructs

A cDNA encoding the full-length Nherf1 (NM_012030) was obtained from the mouse inner ear cDNAs, and inserted into the pcDNA3.1 vector. The cDNAs encoding fragments of cadherin-23 were transferred into appropriate vectors as follows. The cDNA encoding the intracellular region of the cadherin-23 isoform that contains the exon 68-encoded fragment (CDH23+ex68, NM-022124; amino acid residues 3086-3354) was inserted into pCMV-tag3B; and the recombinant cDNA encoding a chimera composed of the extracellular and transmembrane domains of human E-cadherin fused to the cytoplasmic domain of human cadherin-23 lacking the alternative exon 68-encoded fragment (NP_001165405, amino acid residues 847-079) was ligated into pCDNA3.1 (3). A QuikChange XL site-directed mutagenesis kit (Stratagene) was used to delete the segment encoding the last nine amino acid residues of CDH23+ex68 (pCMV-tag3B).

Immunofluorescence and electron microscopy analyses

The distribution of Nherf1 was studied in RJ Swiss mice (Janvier Labs, France). Embryonic day 0 (E0) was determined by vaginal plug detection, and the day of birth was defined as P0. *Nherf1*$^{-/-}$ mice (C57BL/6J background) (4), *Nherf2*$^{-/-}$ mice (5), and *Cdh23*$^{v2j/v2j}$ mice (6) were used. Experiments with animals were carried out using protocols approved by the Animal Use Committee of INSERM and Institut Pasteur.

LLC–PK1–CL4 cells derived from pig kidney (gift from J.R. Bartles, Northwestern University Feinberg School of Medicine, USA) were used as previously described (7). Samples (whole mount preparations of the organ of Corti, cryosections, isolated hair cells, or LLC-PK cells on glass coverslips) were processed for immunofluorescence as previously described (8). Briefly, after blocking in 20% goat serum in phosphate-buffered saline (PBS), and overnight incubation with the primary antibody, sections were rinsed in PBS, incubated with appropriate secondary antibodies for 1 hour at room temperature, and counterstained with DAPI. Images were collected using a Zeiss LSM510 Meta confocal microscope.

For scanning electron microscopy, inner ears were fixed in 2.5% glutaraldehyde in 0.1 M phosphate buffer (pH 7.3) for 2 hours at room temperature. The samples were washed several times with the buffer alone, and cochlear sensory epithelia were finely dissected and processed using the osmium tetroxide/thiocarbohydrazide (OTOTO) method, as previously described (9).

For immunoelectron microscopy, fixed specimens were incubated in pure LR White overnight at room temperature, processed as described (6), and studied under a transmission electron microscope (H-7100, HITACHI, Japan).

The anti-Nherf1 polyclonal antibody (Abcam) was raised against an internal peptide (amino acid residues 286-302) located between the PDZ2 and EB domains of the human protein. Its specificity was verified by immunofluorescence experiments using *Nherf1*$^{-/-}$ mice as negative controls (Supplementary Fig. S2).

The following primary antibodies were used: affinity-purified rabbit polyclonal antibodies against cadherin-23 (3), anti-stereocilin (10), anti-Nherf2 (HPA001672, Sigma), mouse anti-acetylated tubulin (Sigma), and mouse anti-V5-tag (Invitrogen). TRITC-phalloidin (Sigma) and DAPI (1 µg/ml; Sigma) were used to label F-actin and cell nuclei, respectively.

Kinocilium deviation analysis

The deviation of the kinocilium in the outer hair cells at the cochlear base was determined by measuring the angle formed by two crossing lines as described previously (6). The first line was drawn mediolaterally along the symmetry/PCP axis of the cell, thereby running through the expected position of the kinocilium. The second line was drawn between the center of the hair cell surface and the observed position of the kinocilium. Data were

analyzed with the Excel software (Microsoft Office), and Student's *t*-test was used to determine the statistical significance of differences.

In vivo auditory tests

To test hearing, distortion product otoacoustic emissions (DPOAEs), auditory brainstem responses (ABRs), cochlear microphonic (CM) electrical potential, and compound action potentials (CAPs) were recorded in anesthetized mice, and analyzed as described elsewhere (10, 11). Animals were anesthetized with a mixture of ketamine (150 mg/kg) and levomepromazine (2 mg/kg), with additional half doses given every 30 min. Their temperature was kept at 37 °C with a regulated heating blanket.

For DPOAE measurements, f1 and f2 stimuli were carefully applied through different earphones and tubing to avoid nonlinear interactions on earphone membranes. Only the cubic difference tone at $2f_1$-f_2, the most prominent one from the ear (12), was detected. This DPOAE comes mainly from the place where there is maximum overlap between basilar membrane vibrations to f_1 and f_2, i.e., near the place tuned to f_2. Therefore, the $2f_1$-f_2 DPOAE was plotted against f_2. The f_2 frequency was swept from 5 to 32 kHz in $1/8^{th}$ octave steps, with f_1 chosen such that the frequency ratio f_2/f_1 was 1.20. The intensities of the two tonal stimuli at f_1 and f_2 were the same, from 20 to 80 dB SPL in 5 dB steps. We used an IHS system (IHS, Miami, FL, USA) driven by SmartOAE software (IHS) in the growth-function mode, between 5 and 32 kHz. Measurements were extended above 32 kHz, to f_2 = 40 kHz, using a pair of waveform generators (Wavetek 70), and the resulting sound in the ear canal was collected by the IHS microphone, while the $2f_1$-f_2 DPOAE amplitude was measured by an FFT analyzer (OnoSokki). The DPOAE threshold was defined as the weakest stimulus eliciting a DPOAE significantly above the background noise level, estimated from the spectral lines closest to $2f_1$-f_2 in the 0.5 s sound samples collected in the ear canal.

For CAP measurements, a Teflon-coated silver-wire electrode was surgically inserted into the round-window niche, with the negative and ground electrodes subcutaneously placed on the skull and neck regions. The electrocochleogram was collected by a Grass preamplifier (gain x10,000) and numerically averaged (CED 1401+ processor) in synchrony with the stimulus (x32). For ABR recordings, three steel electrodes were inserted (negative and ground as for CAP measurements, and the positive in the mastoid region). The electroencephalogram was collected by the preamplifier with a x100,000 gain, and numerically averaged over 256 epochs.

The acoustic system that generated the tone-bursts for ABR and CAP measurements was controlled for the spectrum and level of onset and offset transient artifacts. These artifacts arise whenever a short, high-frequency voltage burst at frequency f drives an earphone. In ears with a large difference in sensitivity between high- and low-frequency regions, the low-frequency spectral splatter induced by these transients must not be large enough to trigger synchronous neuronal responses from the cochlear region tuned to low frequencies. If, at the same time, the energy of the main spectral peak at f does not exceed the threshold of the cochlear place tuned to it, the ABR and CAP would represent responses to the low-frequency artifact, and thus not be representative of the cochlear sensitivity to f. Likewise, masking TCs would display a dip at low frequencies, because low-frequency maskers would be most efficient at masking an artifactual CAP.

For both ABRs and CAP, the sound stimuli used were tone-bursts produced by a Wavetek-70 arbitrary waveform generator (2-period rise and decay times, 16-period plateau) and sent to a Radioshack tweeter (40-1376, 8 Ohm – 70 W) connected to a conical tip. Tone-burst frequencies were in the range 5 to 40 kHz. At every frequency, the threshold-searching procedure could apply sound intensities from 10 to 115 dB SPL in 2 to 5 dB steps. *In situ* measurements of this setup (probe microphone PCB-Larson-Davis ¼ inch 2520, preamplifier PCB 480C02) connected to a frequency analyzer (Adobe Audition v.1.5)) indicated a 45 dB difference in the intensities of the main spectral peak of a 32 kHz tone burst and of its accompanying, low-frequency onset click (Fig. S8A). The acoustic spectra of 20 kHz tone bursts were similar. The difference was 45 dB regardless of the intensity of the main stimulus between 65 dB and 105 SPL, and this indicates that the growth of the artifact due to spectral splatter is linear. In masking-tuning experiments, the continuous masking tone (being continuous, it is not subject to spectral splatter) was sent through an independent electronic and acoustic channel (a second Radioshack earphone connected to the ear via a Y-shaped tube). Spectral analysis of the sound measured *in situ* indicated that there was no nonlinear interaction between masker and tone-burst.

ABR and CAP thresholds were defined as the sound level producing the smallest detectable wave, verified as reproducible within 2 dB. For CAP masking tuning curves (TCs), the probe sound was a tone-burst at a selected frequency, emitted 5 to 10 dB above the detection threshold, such that the waveform was easily visible. The frequency of the interfering continuous tone was swept over a three-octave range encompassing the probe frequency. The masking criterion from which the masking TC was built was a reduction of 50 % of the probe CAP amplitude due to the presentation of the masker tone. For growth-of-

masking studies, the probe level was increased in 5 dB steps from about 10 dB above detection threshold up to at least 20 dB louder.

Statistical significance was tested with either Student's *t* test or two-way analysis of variance coupled to the Bonferroni post-hoc test (2-way ANOVA). For all statistical tests, the limit of significance was set at $p<0.05$.

References

1. Robles L & Ruggero MA (2001) Mechanics of the mammalian cochlea. *Physiol. Rev.* 81(3):1305-1352.
2. Verpy E*, et al.* (2000) A defect in harmonin, a PDZ domain-containing protein expressed in the inner ear sensory hair cells, underlies Usher syndrome type 1C. *Nature Genet.* 26(1):51-55.
3. Boëda B*, et al.* (2002) Myosin VIIa, harmonin, and cadherin 23, three Usher I gene products, cooperate to shape the sensory hair cell bundle. *EMBO J.* 21(24):6689-6699.
4. Morales FC, Takahashi Y, Kreimann EL, & Georgescu MM (2004) Ezrin-radixin-moesin (ERM)-binding phosphoprotein 50 organizes ERM proteins at the apical membrane of polarized epithelia. *Proc. Natl Acad. Sci. USA* 101(51):17705-17710.
5. Singh AK*, et al.* (2009) Differential roles of NHERF1, NHERF2, and PDZK1 in regulating CFTR-mediated intestinal anion secretion in mice. *J. Clin. Invest.* 119(3):540-550.
6. Lefèvre G*, et al.* (2008) A core cochlear phenotype in USH1 mouse mutants implicates fibrous links of the hair bundle in its cohesion, orientation and differential growth. *Development* 135(8):1427-1437.
7. Zheng L, Zheng J, Whitlon DS, Garcia-Anoveros J, & Bartles JR (2010) Targeting of the hair cell proteins cadherin 23, harmonin, myosin XVa, espin, and prestin in an epithelial cell model. *J. Neurosci.* 30(21):7187-7201.
8. Legendre K, Safieddine S, Kussel-Andermann P, Petit C, & El-Amraoui A (2008) αII/βV spectrin bridges the plasma membrane and cortical lattice in the lateral wall of auditory outer hair cells. *J. Cell Sci.* 121:3347-3356.
9. Furness DN, Katori Y, Nirmal Kumar B, & Hackney CM (2008) The dimensions and structural attachments of tip links in mammalian cochlear hair cells and the effects of exposure to different levels of extracellular calcium. *Neuroscience* 154(1):10-21.
10. Verpy E*, et al.* (2008) Stereocilin-deficient mice reveal the origin of cochlear waveform distortions. *Nature* 456(7219):255-258.
11. Le Calvez S, Avan P, Gilain L, & Romand R (1998) CD1 hearing-impaired mice. I: Distortion product otoacoustic emission levels, cochlear function and morphology. *Hear. Res.* 120(1-2):37-50.
12. Avan P, Büki B, & Petit C (2013) Auditory Distortions: Origins and Functions. *Physiol. rev.* 93(4):1563-1619.

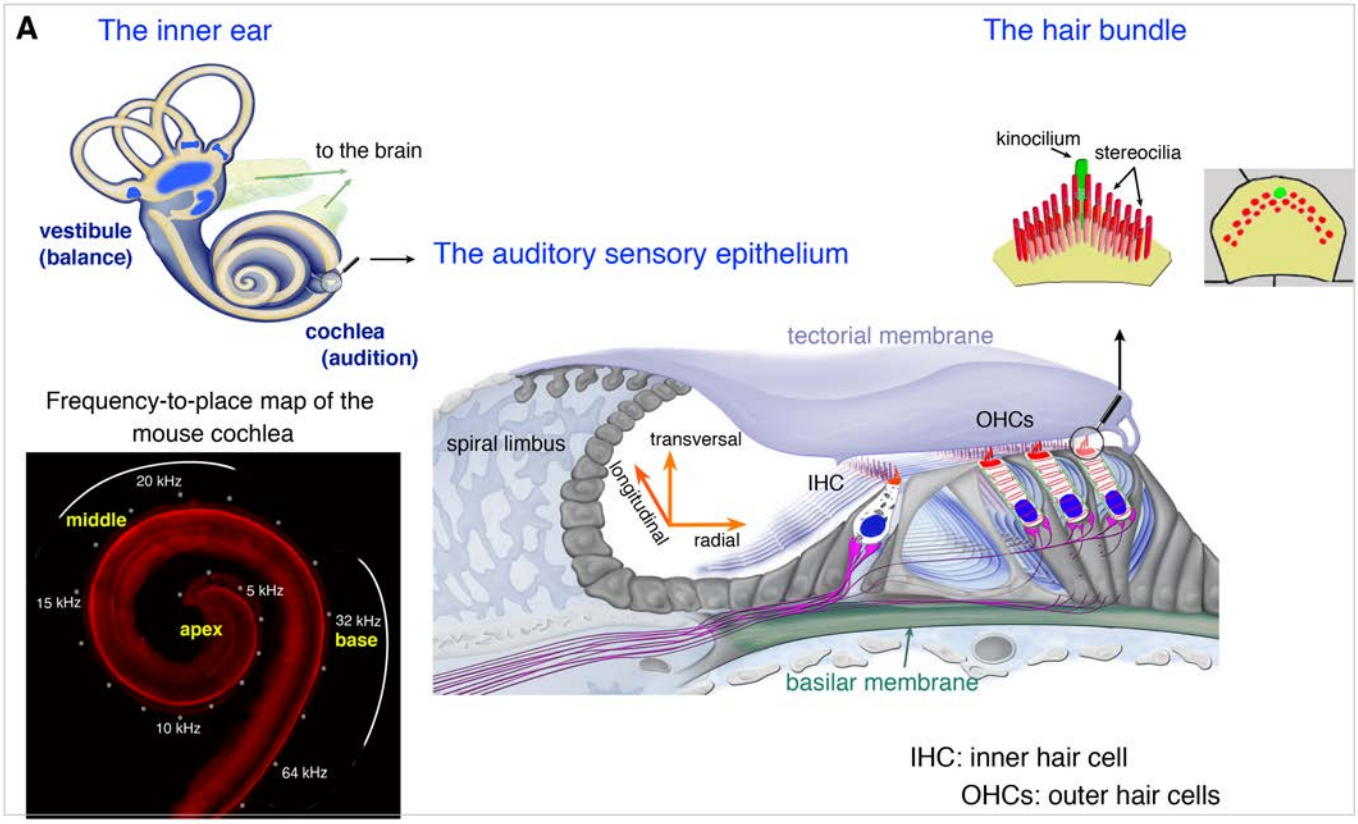
A
The inner ear
to the brain
vestibule (balance)
cochlea (audition)
The auditory sensory epithelium
Frequency-to-place map of the mouse cochlea
20 kHz
middle
15 kHz
5 kHz
apex
32 kHz
base
10 kHz
64 kHz
The hair bundle
kinocilium
stereocilia
tectorial membrane
spiral limbus
transversal
longitudinal
radial
IHC
OHCs
basilar membrane
IHC: inner hair cell
OHCs: outer hair cells

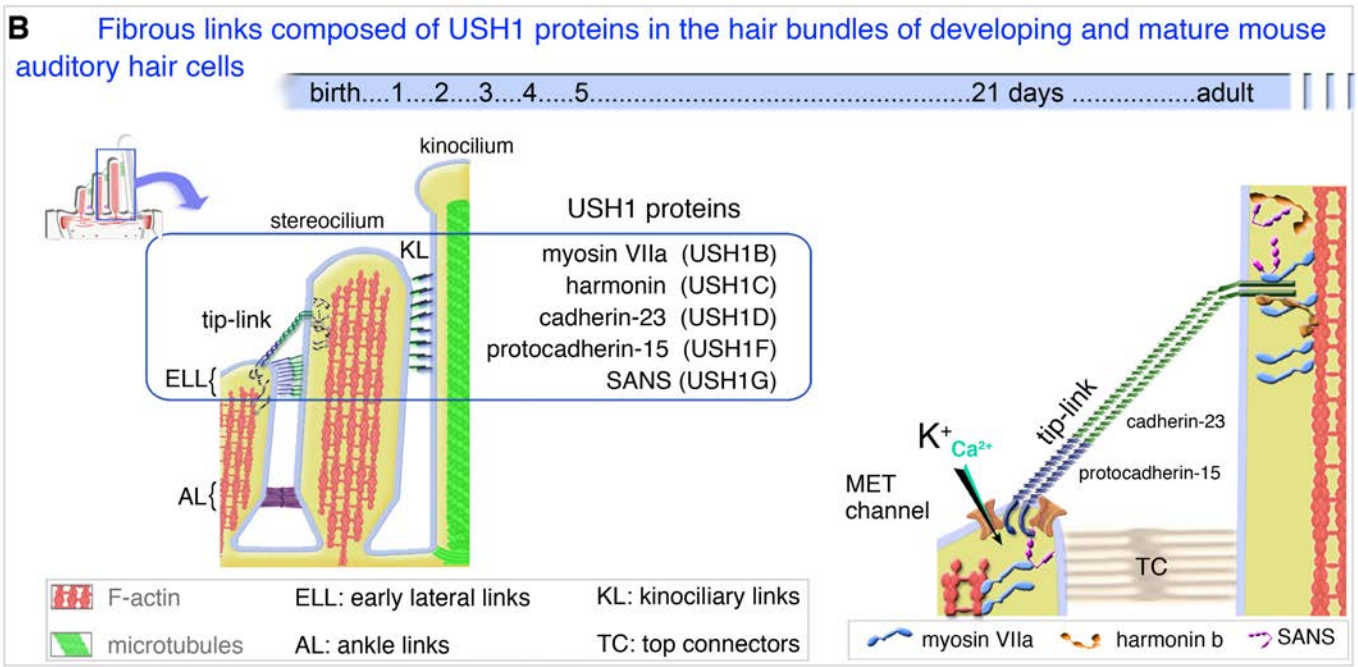
B
Fibrous links composed of USH1 proteins in the hair bundles of developing and mature mouse auditory hair cells
birth....1....2....3....4.....5.....21 days .....adult
kinocilium
stereocilium
KL
tip-link
ELL
AL
USH1 proteins
myosin VIIa (USH1B)
harmonin (USH1C)
cadherin-23 (USH1D)
protocadherin-15 (USH1F)
SANS (USH1G)
F-actin
microtubules
ELL: early lateral links
AL: ankle links
KL: kinociliary links
TC: top connectors
K+
Ca2+
MET channel
tip-link
cadherin-23
protocadherin-15
TC
myosin VIIa
harmonin b
SANS

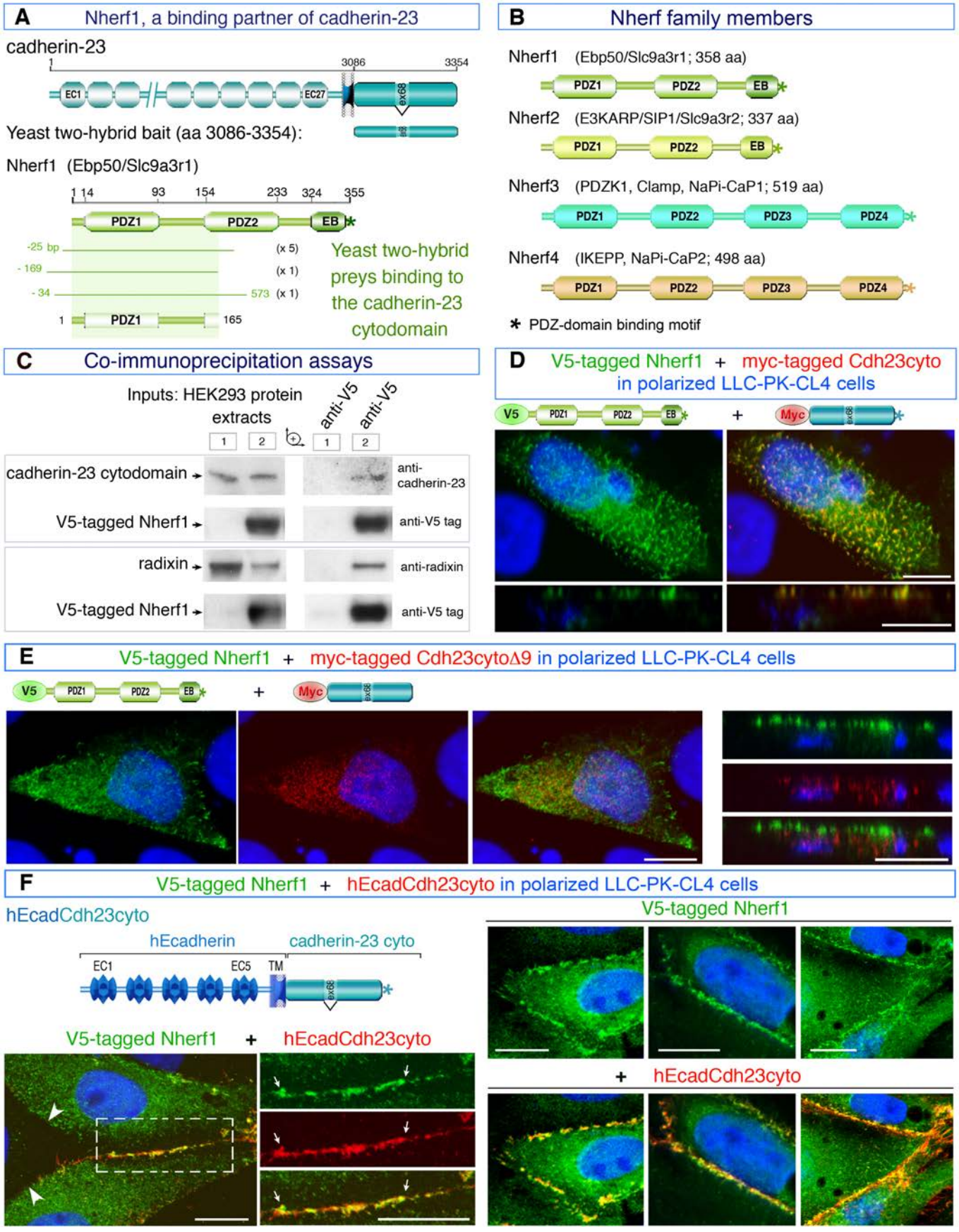
A Nherf1, a binding partner of cadherin-23
cadherin-23
1
3086
3354
EC1
EC27
ex68
Yeast two-hybrid bait (aa 3086-3354):
Nherf1 (Ebp50/Slc9a3r1)
1 14 93 154 233 324 355
PDZ1
PDZ2
EB
-25 bp (x 5)
- 169 (x 1)
- 34 573 (x 1)
1 PDZ1 165
Yeast two-hybrid preys binding to the cadherin-23 cytodomain
B Nherf family members
Nherf1 (Ebp50/Slc9a3r1; 358 aa)
PDZ1 PDZ2 EB
Nherf2 (E3KARP/SIP1/Slc9a3r2; 337 aa)
PDZ1 PDZ2 EB
Nherf3 (PDZK1, Clamp, NaPi-CaP1; 519 aa)
PDZ1 PDZ2 PDZ3 PDZ4
Nherf4 (IKEPP, NaPi-CaP2; 498 aa)
PDZ1 PDZ2 PDZ3 PDZ4
* PDZ-domain binding motif
C Co-immunoprecipitation assays
Inputs: HEK293 protein extracts
anti-V5
anti-V5
1 2 1 2
cadherin-23 cytodomain
anti-cadherin-23
V5-tagged Nherf1
anti-V5 tag
radixin
anti-radixin
V5-tagged Nherf1
anti-V5 tag
D V5-tagged Nherf1 + myc-tagged Cdh23cyto in polarized LLC-PK-CL4 cells
V5 PDZ1 PDZ2 EB + Myc ex68
E V5-tagged Nherf1 + myc-tagged Cdh23cytoΔ9 in polarized LLC-PK-CL4 cells
V5 PDZ1 PDZ2 EB + Myc ex68
F V5-tagged Nherf1 + hEcadCdh23cyto in polarized LLC-PK-CL4 cells
hEcadCdh23cyto
hEcadherin
cadherin-23 cyto
EC1
EC5
TM
ex68
V5-tagged Nherf1 + hEcadCdh23cyto
V5-tagged Nherf1
+ hEcadCdh23cyto

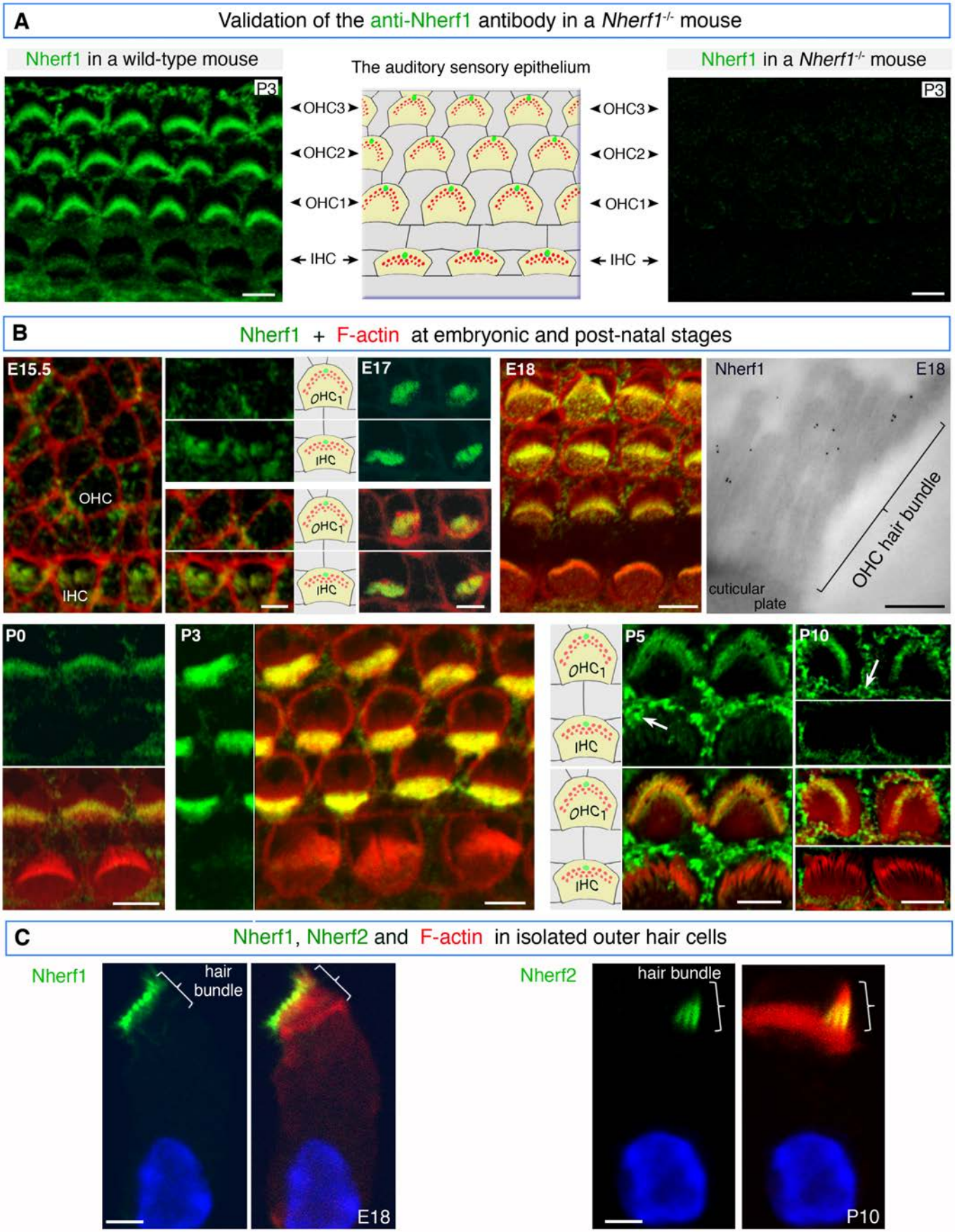
A
Validation of the anti-Nherf1 antibody in a Nherf1-/- mouse
Nherf1 in a wild-type mouse
P3
The auditory sensory epithelium
OHC3
OHC2
OHC1
IHC
Nherf1 in a Nherf1-/- mouse
P3
B
Nherf1 + F-actin at embryonic and post-natal stages
E15.5
OHC
IHC
E17
E18
Nherf1
E18
OHC hair bundle
cuticular plate
P0
P3
P5
P10
C
Nherf1, Nherf2 and F-actin in isolated outer hair cells
Nherf1
hair bundle
E18
Nherf2
hair bundle
P10

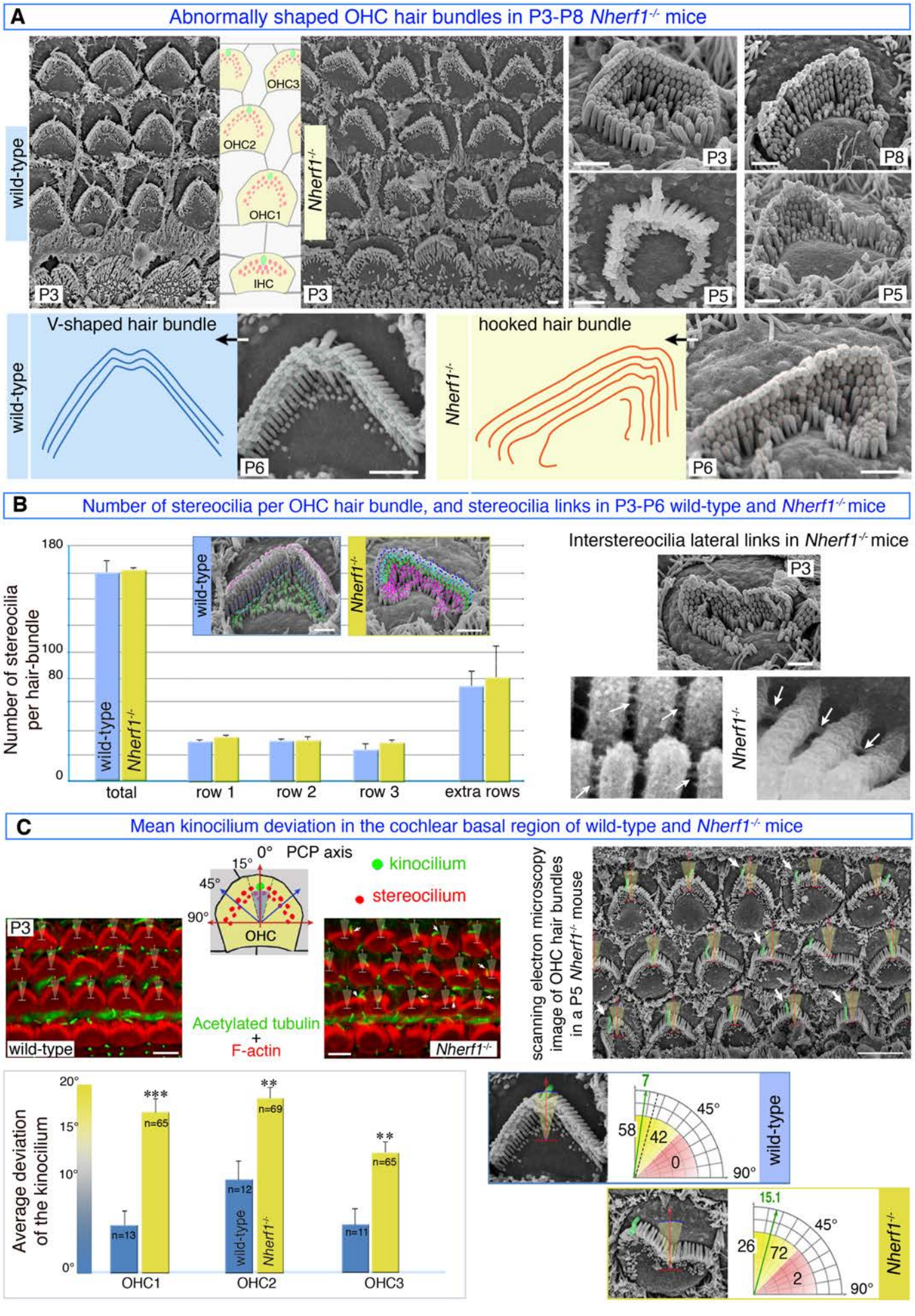
A
Abnormally shaped OHC hair bundles in P3-P8 Nherf1-/- mice
wild-type
Nherf1-/-
OHC3
OHC2
OHC1
IHC
P3
P3
P8
P5
P5
V-shaped hair bundle
hooked hair bundle
P6
P6
B
Number of stereocilia per OHC hair bundle, and stereocilia links in P3-P6 wild-type and Nherf1-/- mice
Number of stereocilia per hair-bundle
180
100
80
0
wild-type
Nherf1-/-
total
row 1
row 2
row 3
extra rows
Interstereocilia lateral links in Nherf1-/- mice
P3
Nherf1-/-
C
Mean kinocilium deviation in the cochlear basal region of wild-type and Nherf1-/- mice
0° PCP axis
15°
45°
90°
OHC
kinocilium
stereocilium
P3
wild-type
Acetylated tubulin
+
F-actin
Nherf1-/-
scanning electron microscopy image of OHC hair bundles in a P5 Nherf1-/- mouse
Average deviation of the kinocilium
20°
15°
10°
0°
***
n=65
n=13
**
n=69
n=12
**
n=65
n=11
wild-type
Nherf1-/-
OHC1
OHC2
OHC3
7
58
42
0
45°
90°
wild-type
15.1
26
72
2
45°
90°
Nherf1-/-

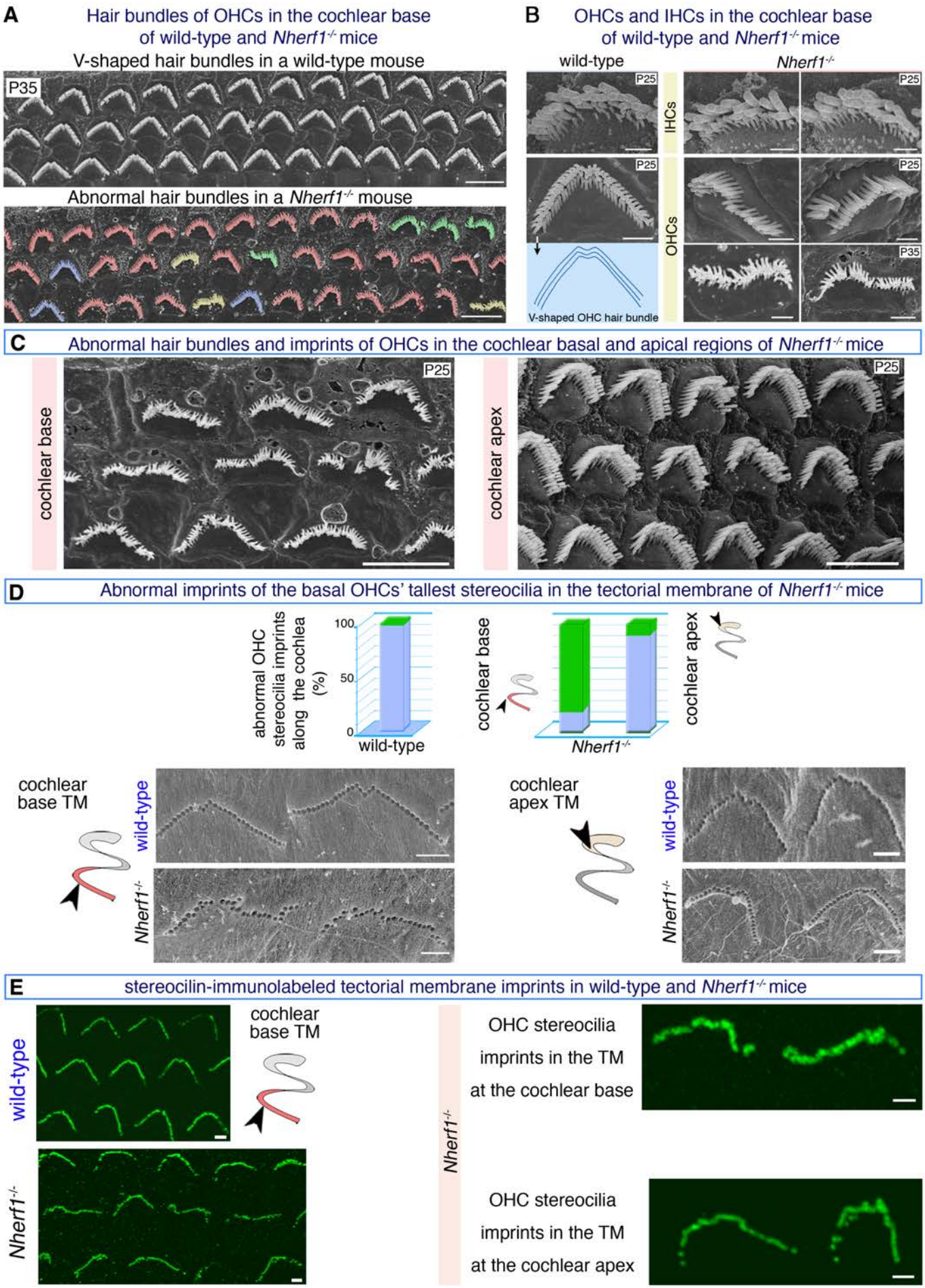
A
Hair bundles of OHCs in the cochlear base of wild-type and Nherf1-/- mice
V-shaped hair bundles in a wild-type mouse
P35
Abnormal hair bundles in a Nherf1-/- mouse
B
OHCs and IHCs in the cochlear base of wild-type and Nherf1-/- mice
wild-type
Nherf1-/-
P25
P35
IHCs
OHCs
V-shaped OHC hair bundle
C
Abnormal hair bundles and imprints of OHCs in the cochlear basal and apical regions of Nherf1-/- mice
cochlear base
cochlear apex
P25
D
Abnormal imprints of the basal OHCs' tallest stereocilia in the tectorial membrane of Nherf1-/- mice
abnormal OHC stereocilia imprints along the cochlea (%)
100
50
0
wild-type
cochlear base
cochlear apex
Nherf1-/-
cochlear base TM
cochlear apex TM
wild-type
Nherf1-/-
E
stereocilin-immunolabeled tectorial membrane imprints in wild-type and Nherf1-/- mice
wild-type
Nherf1-/-
cochlear base TM
OHC stereocilia imprints in the TM at the cochlear base
OHC stereocilia imprints in the TM at the cochlear apex

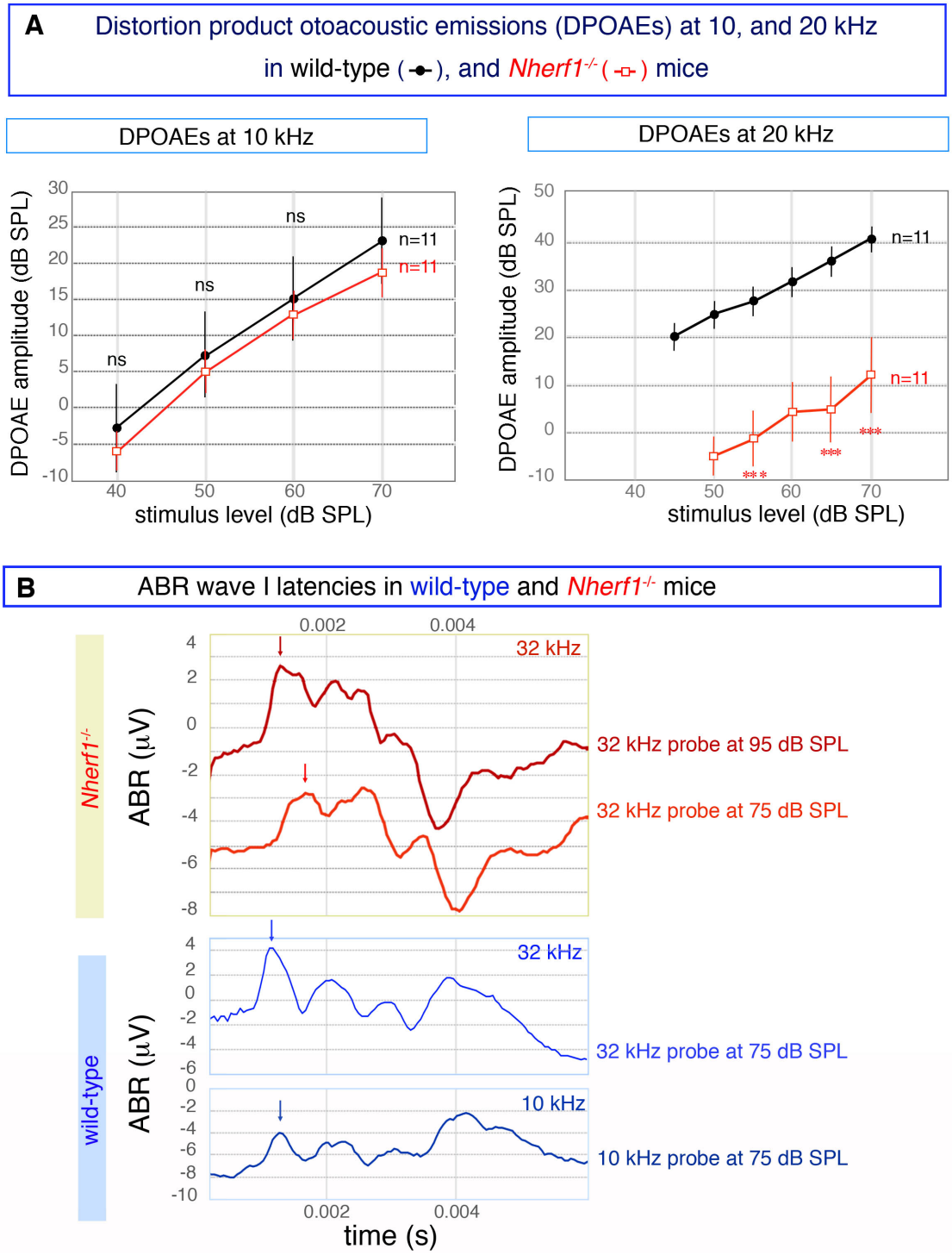
A
Distortion product otoacoustic emissions (DPOAEs) at 10, and 20 kHz
in wild-type (●), and Nherf1-/- (□) mice
DPOAEs at 10 kHz
DPOAEs at 20 kHz
DPOAE amplitude (dB SPL)
stimulus level (dB SPL)
ns
n=11
***
B
ABR wave I latencies in wild-type and Nherf1-/- mice
Nherf1-/-
wild-type
ABR (μV)
time (s)
32 kHz
10 kHz
32 kHz probe at 95 dB SPL
32 kHz probe at 75 dB SPL
10 kHz probe at 75 dB SPL

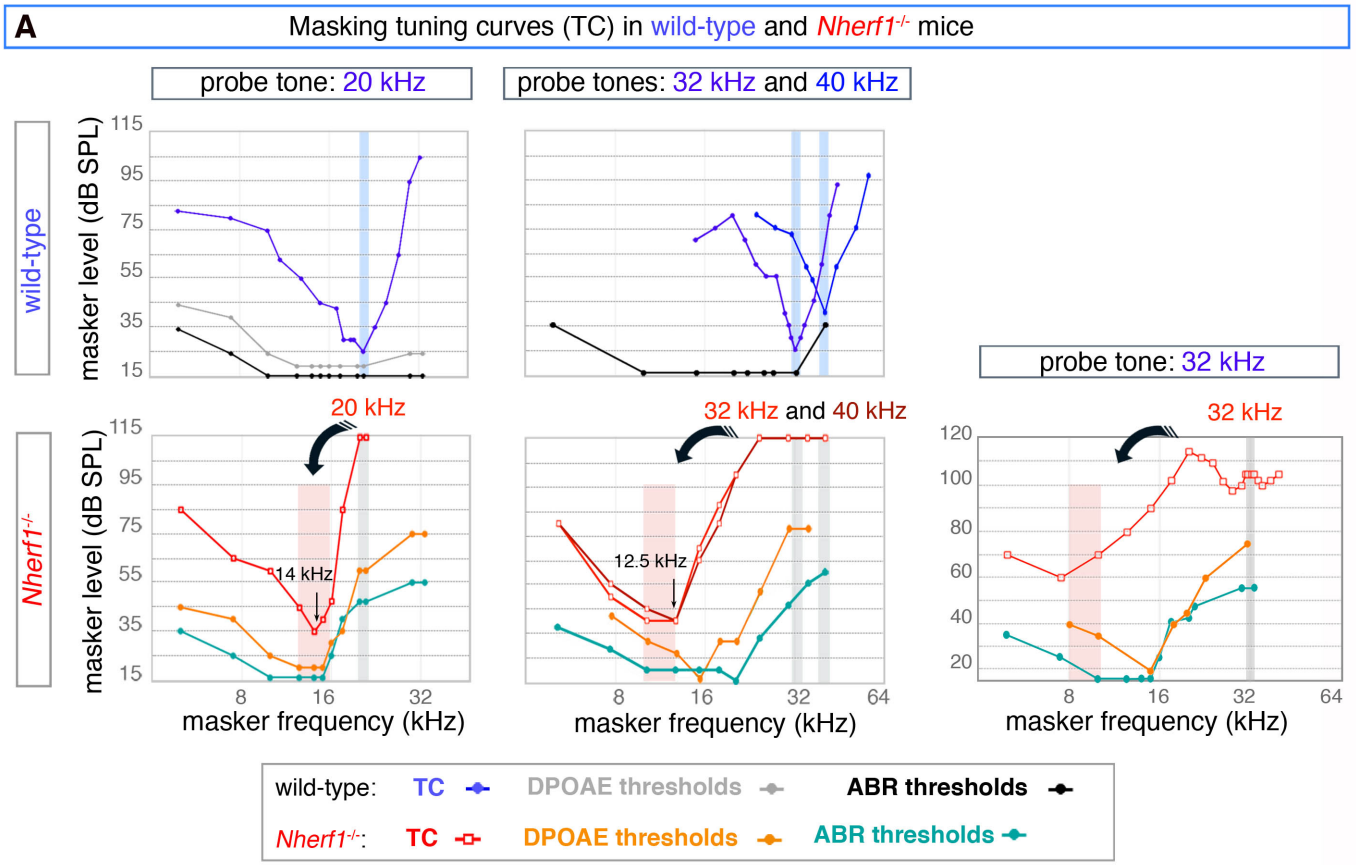
A
Masking tuning curves (TC) in wild-type and Nherf1-/- mice
probe tone: 20 kHz
probe tones: 32 kHz and 40 kHz
probe tone: 32 kHz
wild-type
Nherf1-/-
masker level (dB SPL)
20 kHz
32 kHz and 40 kHz
32 kHz
14 kHz
12.5 kHz
masker frequency (kHz)
wild-type: TC DPOAE thresholds ABR thresholds
Nherf1-/-: TC DPOAE thresholds ABR thresholds

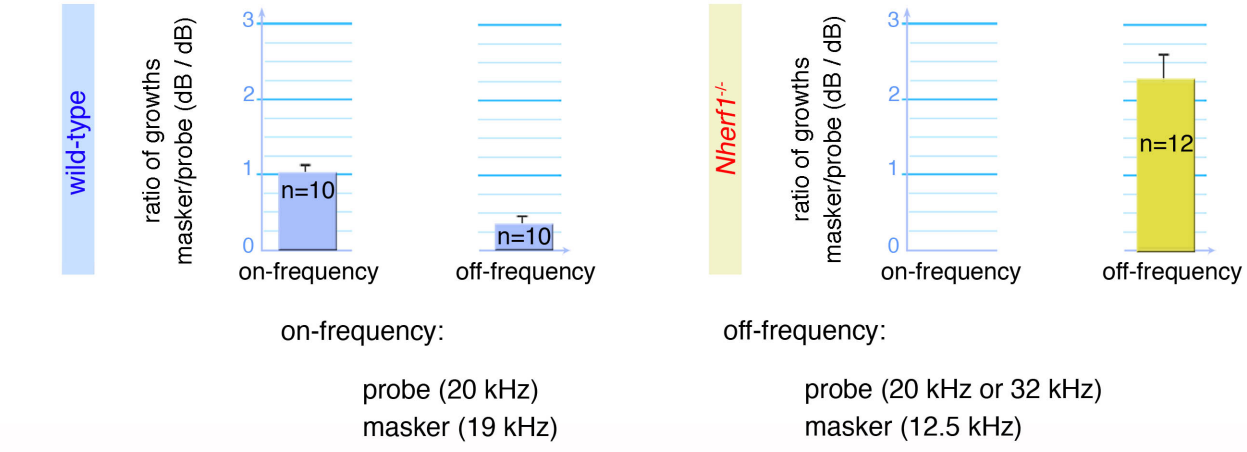
B
Growth of masking for on- and off-frequency conditions in wild-type and Nherf1-/- mice
wild-type
Nherf1-/-
ratio of growths masker/probe (dB / dB)
n=10
n=10
n=12
on-frequency
off-frequency
on-frequency:
probe (20 kHz)
masker (19 kHz)
off-frequency:
probe (20 kHz or 32 kHz)
masker (12.5 kHz)

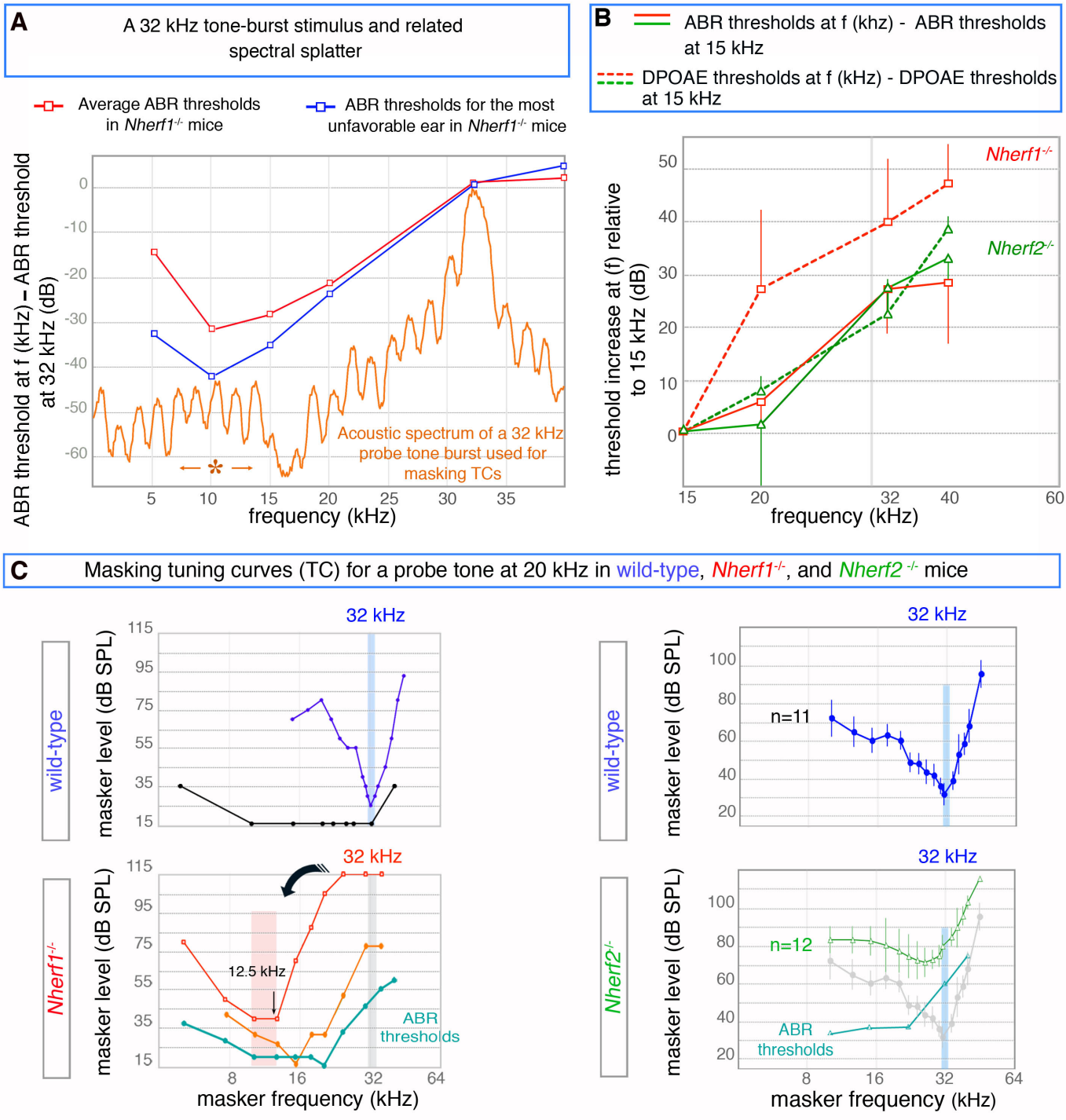
A
A 32 kHz tone-burst stimulus and related spectral splatter
Average ABR thresholds in Nherf1-/- mice
ABR thresholds for the most unfavorable ear in Nherf1-/- mice
ABR threshold at f (kHz) – ABR threshold at 32 kHz (dB)
Acoustic spectrum of a 32 kHz probe tone burst used for masking TCs
frequency (kHz)
B
ABR thresholds at f (khz) - ABR thresholds at 15 kHz
DPOAE thresholds at f (kHz) - DPOAE thresholds at 15 kHz
threshold increase at (f) relative to 15 kHz (dB)
Nherf1-/-
Nherf2-/-
frequency (kHz)
C
Masking tuning curves (TC) for a probe tone at 20 kHz in wild-type, Nherf1-/-, and Nherf2-/- mice
wild-type
masker level (dB SPL)
32 kHz
Nherf1-/-
12.5 kHz
ABR thresholds
masker frequency (kHz)
n=11
Nherf2-/-
n=12

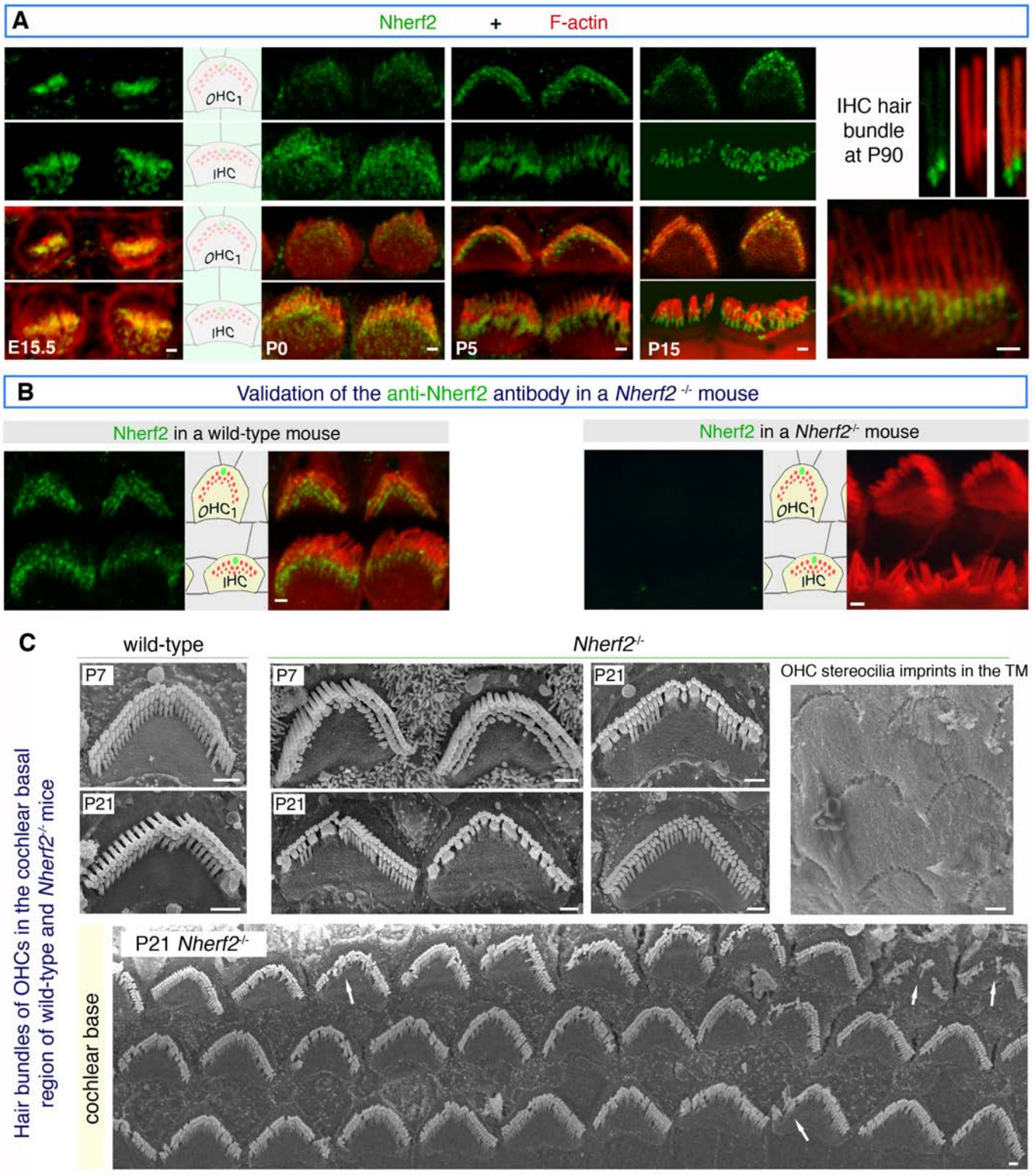
A
Nherf2 + F-actin
OHC1
IHC
E15.5
P0
P5
P15
IHC hair bundle at P90
B
Validation of the anti-Nherf2 antibody in a Nherf2 -/- mouse
Nherf2 in a wild-type mouse
Nherf2 in a Nherf2-/- mouse
C
wild-type
Nherf2-/-
P7
P21
OHC stereocilia imprints in the TM
Hair bundles of OHCs in the cochlear basal region of wild-type and Nherf2-/- mice
cochlear base
P21 Nherf2-/-